Metabolic Engineering of Cyanobacteria for Increased Product Formation

By

Adeola Oluyemisi Adebiyi

Thesis

Submitted to the Faculty of the

Graduate School of Vanderbilt University

in partial fulfillment of the requirements

for the degree of

MASTER OF SCIENCE

in

Chemical Engineering

August, 2015

Nashville, Tennessee

Approved:

Jamey D. Young, Ph.D.

Scott Guelcher, Ph.D.

ACKNOWLEDGEMENTS

I would first like to thank the Lord for bringing me to this city and university and for allowing me to experience so much and to mature during my time here.

I would like to acknowledge my department and former and current department heads Peter Pintauro and Kane Jennings for allowing me the opportunity to pursue a higher degree. I wish to express my appreciation for and to my advisor Jamey Young for his guidance. Your breadth of knowledge and continuous hunger for learning is inspiring. I recognize my lab mates, especially Lara Jazmin, and our research assistant Irina Trenary for all of their help, and give special thanks to my undergraduate student, Victoria Potter. Your enthusiasm and desire to help were invaluable.

I would like to recognize members of my thesis committee, Scott Guelcher and Clare McCabe and Carl Johnson of Biological Sciences. I would like to further thank Dr. Johnson and members of his lab, Drs. Tetsuya Mori, Yao Xu, and Peijun Ma, for all of their assistance and expertise with cyanobacteria. Thank you, Dr. Johnson, for your inquisitive and frank nature.

Special thanks go to both my natural family and my Nashville family. Thank you all for your support and continued encouragement throughout my endeavors. I would like to mention my sister AdeDoyin Adebiyi for pretending to understand my research as well as Martha Wall, her little ones, and Courtney A. Mitchell for their proofing help and constant support.

I end with acknowledgement of my funding sources: the U.S. Department of Education's Graduate Assistance in Areas of National Need award (P200A090323), Vanderbilt's Provost Graduate Fellowship, and for the project, the U.S. Department of Energy Award DE-SC008118.

And finally, Anchor Down.

TABLE OF CONTENTS

Page

LIST OF TABLES

LIST OF FIGURES

CHAPTER I

INTRODUCTION

Cyanobacteria have recently garnered attention as a renewable production source for fuels and chemicals. Manipulation of endogenous metabolic pathways has yielded hydrogen (Dutta et al. 2005; Masukawa et al. 2010), ethanol (Deng and Coleman 1999), higher alcohols (Oliver et al. 2013; Varman et al. 2013), fatty acids and fatty alcohols (Liu et al. 2011; Yao et al. 2014), and several other products (Ducat et al. 2011; Quintana et al. 2011). The appeal of these prokaryotes as "mini factories" lies in their ability to capture CO_2 from the atmosphere. This decreases the feedstock cost and provides a secondary level of environmental benefit (Kumar et al. 2011).

A primary limitation of industrial use of cyanobacteria is the high cost of culture vessels. Open raceway ponds are a low-cost option. The ponds are supplied with nutrients and water either continuously or in batch. However, the open-atmosphere design leaves the culture susceptible to contamination, and the cost of biomass harvesting and product separation is often high. This design remains useful for strains of microalgae with high growth rates or requiring selective growth media, such as high alkalinity or salinity (Hu and Richmond 2013). Ponds may be used for products requiring little further separation, for example, Spirulina, an edible alga (Earthrise®). In this case, the whole cell is dried and pelleted, avoiding the cost of lysing cells and separating the extracted metabolites.

Another system for industrial production of cyanobacteria is the photobioreactor (Sharma et al. 2013). Specific styles differ, but common features include (i) a barrier to prevent outside contamination and provide better control of conditions, (ii) continuous feed of nutrients, including

CO_2 and pH adjusters, and (iii) a light source, either directly from the sun or from artificial lights. While these allow for greater control than open raceway ponds, the tradeoff is the higher costs in purchase and maintenance of these specialized reactors.

Other drawbacks limiting the industrial implementation of cyanobacteria are low production titers and cell biomass production, especially when compared to other industrial microbes, such as *Escherichia coli* and yeast. For example, a 2,3-butanediol production pathway was introduced into both *E. coli* and a strain of cyanobacteria, *Synechococcus elongatus* sp. PCC 7942. Yield in *E. coli* peaked at 13.8 g L^{-1} over 40 hours whereas *S. elongatus* yield peaked at 2.38 g L^{-1} over a longer period of 21 days, a difference of almost two orders of magnitude in daily productivity (8.28 g L^{-1} day^{-1} versus 0.11 g L^{-1} day^{-1}) (Oliver et al. 2013). Most of the tools used to address these drawbacks have been adapted from *E. coli*. This causes progress in the industrial application of cyanobacteria to lag further behind the existing platform microbes.

Through metabolic engineering, the cyanobacterial genome can be manipulated to address low cell productivity. Metabolic engineering is an emerging field that emphasizes rational alterations of organismal metabolism through iterative synthesis and analysis steps (Stephanopoulos et al. 1998). Synthesis may involve the overexpression, knockdown, or knockout of an existing gene or the introduction of an exogenous gene into the host of interest to facilitate product formation. These new pathways are introduced to cellular metabolism through recombinant DNA technology. Analysis involves characterizing the strains of interest. The characterized strains are compared to a control strain to determine how to engineer the cells for further improvement.

Strain characterization often includes observing rates of (i) substrate consumption, (ii) growth, and (iii) product formation to compare the effects of genetic alterations. In terms of

carbon flux or flow through the system, substrate consumption is the amount of carbon intake. Growth rate is a measure of carbon metabolized into biomass production. Product formation reflects carbon flux into the desired sink. Additional measurements may be collected to characterize each strain further. Large-scale sets of data used to compare phenotypic responses at various subcellular levels are labeled with the suffix '-omics'. These include data that span broad ranges of cellular metabolism and track changes at the gene, protein, metabolite, or flux levels to observe bulk response to stimuli. The information compiled during characterization is used to identify specific gene targets for further engineering to improve product formation. Further manipulation may include altering the specific genes introduced or removing competing pathways within the cells to further increase productivity.

This project applies metabolic engineering to cyanobacteria. Chapter 2 of this thesis reviews previous work on cyanobacteria using the analytical method of metabolic flux analysis and also the synthesis of two products from the major precursor pyruvate. Chapter 3 probes an analytical model of central carbon metabolism previously applied to cyanobacteria. This study highlights key experimental data for reliable estimation of carbon flux through these critical pathways. One of the key findings from the previous analysis has been applied to a specific strain of aldehyde-producing cyanobacteria in Chapter 4. Strains overexpressing the genes of interest are characterized and compared to determine a new target for further gene engineering to optimize product formation. Chapter 5 provides a conclusion of the work performed for this thesis and suggestions for future direction of this project based on results.

CHAPTER II

LITERATURE REVIEW

MFA in Cyanobacteria

Metabolic flux analysis (MFA) is a useful analysis tool for metabolic engineering. This computational tool has allowed for observation of flux in several platform organisms. MFA is commonly supplemented with labeling experiments to broaden the range of fluxes feasibly estimated and to increase the certainty of the calculations. Following introduction of stable isotopically labeled substrates to cells, the resultant labeling of downstream metabolites provides information used to quantify intracellular fluxes in pathways of interest. Due to recent advances, MFA can be conducted either at metabolic (quasi)steady state or in a more dynamic state of metabolism (Leighty and Antoniewicz 2011). Further, labeling may be measured once the atom labeling has been fully incorporated, in steady-state MFA (Wiechert 2001), or during the transient phase of label incorporation, in isotopically nonstationary MFA (Noh et al. 2007) (Figure 2.1). This first section reviews explorations of ^{13}C MFA in cyanobacteria under metabolic steady state, using both steady-state labeling measurements and also isotopically nonstationary labeling measurements. A summary is provided on previous applications, describing culture conditions with emphasis on the labeled substrate(s) utilized and the resulting shifts in metabolism under the varying conditions.

Steady-state ^{13}C MFA. Steady-state MFA was first applied to *Synechocystis* sp. PCC 6803 to investigate central carbon metabolism under mixotrophic and heterotrophic conditions (Yang et al. 2002a, b, c). The predominant mode of carbon utilization was determined by analyzing

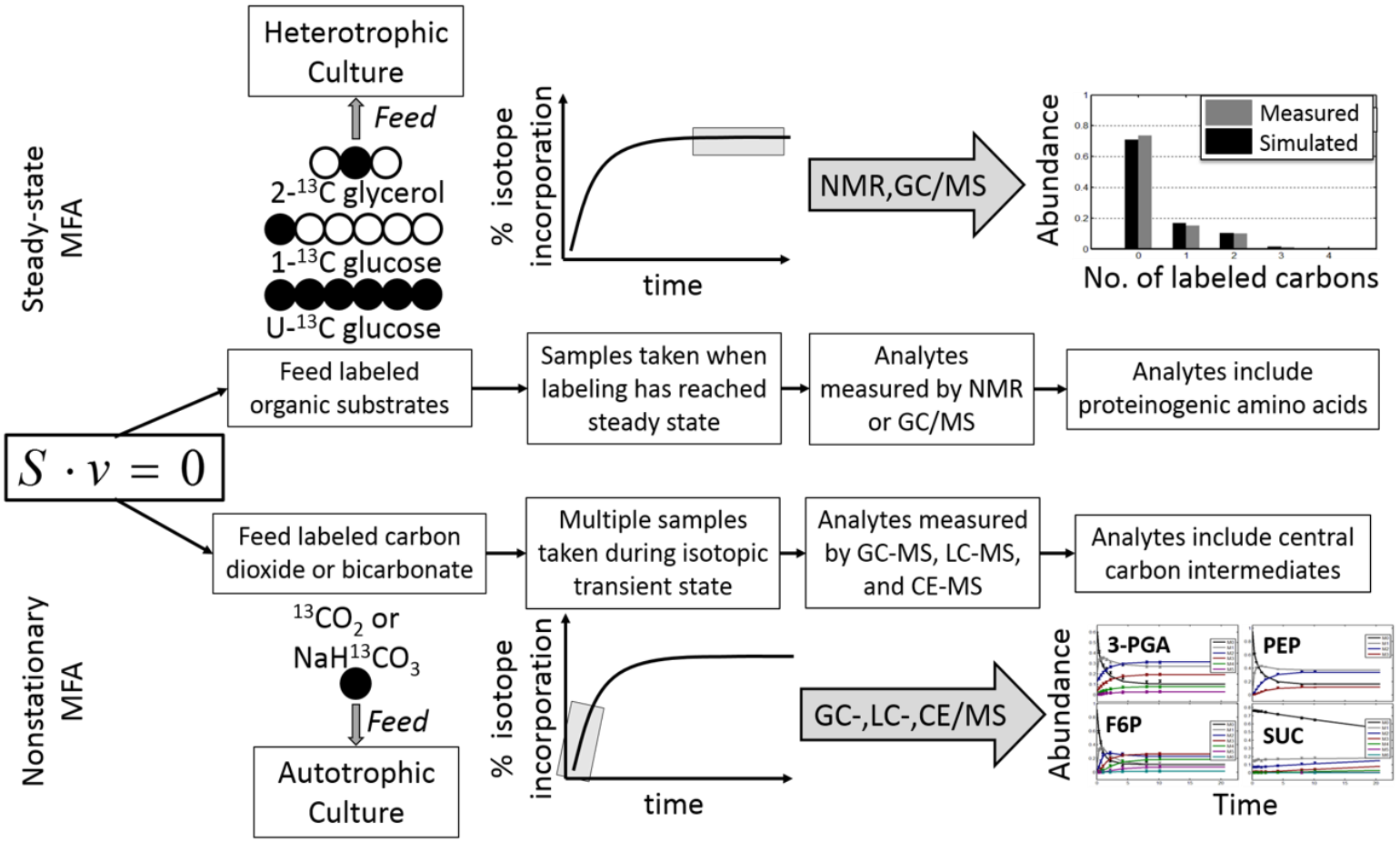

Figure 2.1 – Two primary ^{13}C MFA approaches applied to cyanobacteria. MFA begins with a set of mass balances describing a cell culture at metabolic steady state. Feeding a ^{13}C tracer and measuring isotopomer abundances of intracellular metabolites provides additional information to constrain the flux solution. This involves least-squares regression based on an expanded model that includes both mass and isotopomer balances. Heterotrophic cultures are analyzed by performing steady-state MFA with labeling measurements obtained from ^{13}C-labeled glucose or glycerol tracers. Autotrophic cultures require transient ^{13}C labeling experiments followed by INST-MFA. Abbreviations: ***S***: stoichiometric matrix; ***v***: flux vector. Figure taken from Adebiyi et al. (2014).

metabolite labeling using a mixed feed of 90% unlabeled glucose and 10% fully-labeled [U-$^{13}C_6$] glucose. Heterotrophic cells were found to utilize the oxidative pentose phosphate pathway (oxPPP) almost exclusively for energy production, with more than 90% of the incoming glucose metabolized through this pathway to produce NADPH for growth and respiration. The coupling of NADPH production to oxidative phosphorylation represents a unique respiratory pathway found in cyanobacteria and is believed to compensate for the lack of an intact cyanobacterial TCA cycle (Pelroy et al. 1972). Under mixotrophic conditions, CBB cycle flux was approximately two-fold higher than glucose uptake, fueled by NADPH and ATP production from photosynthetic light reactions. However, flux through RUBP carboxylase/oxygenase (RuBisCO) still only accounted for one-third of the total carbon uptake. A substantial cyclic flux was noted through phosphoenolpyruvate carboxylase (PEPC) and malic enzyme (ME) under both heterotrophic and mixotrophic conditions, which is similar to the pathway of carbon assimilation found in C4 plants.

In addition to their ^{13}C MFA studies, Yang et al. (2002a) compared mRNA transcript levels and protein expressions with pathway fluxes to decipher mechanisms of metabolic regulation. Consistent with their flux results, genes encoding phycobilisomes, RuBisCO, and the CBB-cycle associated *gap2* isoform of glyceraldehyde-3-phosphate dehydrogenase (GAPDH) were all transcriptionally repressed under heterotrophic conditions, while the oxPPP gene *gnd* (gluconate-6-phosphate or G6P ↔ ribulose-5-phosphate or RU5P) was upregulated by about 60%. Conversely, some expression levels did not appear to be in agreement with the flux results, indicating post-translational regulation by cellular redox or metabolite concentrations. Several genes encoding enzymes of central carbon metabolism were largely unaffected by light at the transcriptional level despite dramatic rerouting of flux through these pathways. This work

highlighted the utility of ^{13}C MFA to uncover novel insights about regulatory mechanisms when combined with other '-omics' platforms.

Nakajima et al. (2014) combined ^{13}C MFA with metabolomic and transcriptomic analyses of *Synechocystis* to compare cells grown under mixotrophic conditions and photoheterotrophic conditions. Labeling was achieved by an optimized mix of 70% [1-^{13}C] glucose and 30% [U-^{13}C] glucose while atrazine was added to the photoheterotrophic cultures to inhibit photosynthesis. Samples were taken during the exponential growth phase, and nine proteinogenic amino acids were selected for analysis: alanine, aspartate, glutamate, phenylalanine, glycine, isoleucine, leucine, serine, and valine. A comparison of the fluxes and their 95% confidence intervals showed that over half of the fluxes differed significantly between the two culture conditions. Changes in enzyme expression within these pathways were less dramatic, with most genes differing by less than two-fold between mixotrophic and photoheterotrophic conditions. A six-fold increase in RuBisCO activity was observed under mixotrophic conditions when compared to photoheterotrophic conditions. However, there was no significant change in the levels of RU5P or ribulose-1,5-bisphosphate (RUBP) or in the expression of phosphoribulokinase (RU5P ↔ RUBP) or RuBisCO large and small subunits. OxPPP flux was elevated under photoheterotrophic conditions to compensate for loss of photosynthetically produced NAPDH, but gene expression was again unaffected. In contrast to the previous study of Yang et al. (2002c), some residual oxPPP flux was still detectable under mixotrophic conditions. The authors attributed this to the lower light intensity used in the more recent study (40 μmol m^{-2} s^{-1} vs 125 μmol m^{-2} s^{-1}), consistent with model predictions reported by Shastri and Morgan (2005). The gene that exhibited the largest expression change was *gap1*, which encodes an isoform of GAPDH that is essential for

glycolytic glucose breakdown and was suggested to respond to NADPH levels by shifting carbon flow between glycolysis and oxPPP.

Another recent study by You et al. (2014) confirmed conclusions from previous studies in *Synechocystis* under mixotrophic growth conditions. In addition to ^{13}C MFA, isotope dilution experiments were performed to identify the presence of particular pathways. Cells were fully labeled using $NaH^{13}CO_3$ and [U-^{13}C] glucose. Then unlabeled glyoxylate or glutamate was added to determine the activities of specific reactions. The MFA model yielded evidence of high malic enzyme activity in agreement with the previous analysis by Yang et al. (2002b). OxPPP flux was low under the light- and carbon-sufficient conditions of the early-exponential phase, but labeling in late-exponential phase indicated higher oxPPP activity. You et al. focused particular attention toward elucidating the direction and activity of the TCA cycle. Similar to the flux analysis of Nakajima et al. (2014), this study calculated a zero flux through the glyoxylate shunt. Isotope dilution with glutamate detected carbon flow through α-ketoglutarate to succinate, which was consistent with activity of the α-ketoglutarate decarboxylase bypass pathway recently discovered by Zhang and Bryant (2011). However, ^{13}C MFA verified that flux through this pathway was negligibly small, in agreement with previous MFA studies.

In addition to *Synechocystis*, other strains of cyanobacteria have also become the subject of recent flux profiling experiments. A steady-state ^{13}C labeling study by Feng et al. (2010) investigated the effects of different carbon and nitrogen substrates on the central metabolism of *Cyanothece* sp. ATCC 51142 under continuous light conditions. Three labeled substrates were tested ([U-^{13}C] glucose, [2-^{13}C] glycerol, and [3-^{13}C] pyruvate) in either nitrogen-fixing or nitrogen-sufficient conditions to determine their impacts on growth and amino acid biosynthesis. GC-MS was used to analyze the ^{13}C enrichment of five amino acids: histidine and serine, which

are synthesized from CBB cycle and PPP intermediates; alanine, which is derived from pyruvate; and aspartate and glutamate, which are both TCA cycle derivatives (Figure 2.2). Glycerol addition doubled the specific growth rate under both nitrogen-fixing and nitrogen-sufficient conditions, but neither glucose nor pyruvate enhanced growth in comparison to a control photoautotrophic culture. Consistent with this observation, the contribution of glycerol carbon to amino acid biosynthesis was substantially higher than either glucose or pyruvate. Furthermore, the amino acids histidine, alanine, and serine were completely derived from glycerol carbon under nitrogen-sufficient conditions, indicating a shift to photoheterotrophic growth. This study highlights the use of ^{13}C labeling studies to reveal major pathways of carbon utilization in less-characterized species.

Feng et al. (2010) made extensive use of ^{13}C labeling data to determine the contributions of extracellular carbon substrates to intracellular amino acid pools but did not attempt to estimate intracellular fluxes using rigorous pathway modeling. Another study by Alagesan et al. (2013) provided a more comprehensive flux analysis of *Cyanothece* sp. ATCC 51142 metabolism under similar growth conditions. A comparison of these two studies underscores the effects that culture conditions and measurement availability have on the computed fluxes. Both groups analyzed growth in nitrogen-sufficient and nitrogen-fixing conditions using ^{13}C-labeled glycerol as a carbon source. However, Feng et al. determined that a glycerol-fed culture in nitrogen-replete media exhibited photoheterotrophic growth in the presence of light, while Alagesan et al. observed mixotrophic metabolism under similar conditions. The variation in culture experimental setup likely caused this difference, as the latter group chose a higher light intensity (100 μmol m^{-2} s^{-1} vs. 50 μmol m^{-2} s^{-1}) to avoid light limitation, and the cells were harvested early in the exponential growth phase to maintain sufficient CO_2 availability. Also, a greater number of amino acids were analyzed by Alagesan et al., providing increased redundancy and pathway coverage. This enabled

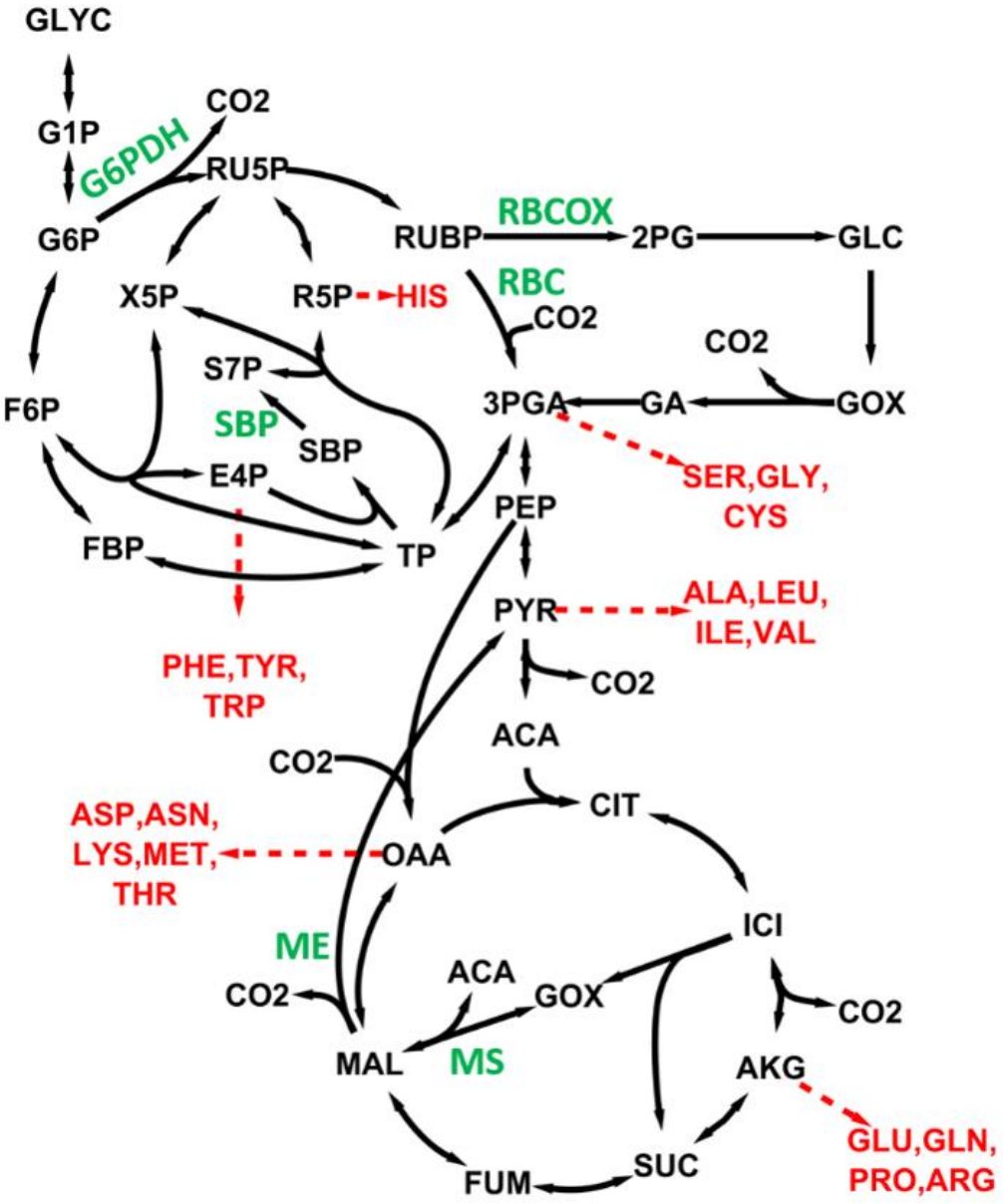

Figure 2.2 – Model for INST-MFA analysis of central carbon metabolism. Pathways include the Calvin-Benson-Bassham cycle and oxidative pentose phosphate, photorespiration, lower glycolysis, and the TCA cycle. The six fluxes used in the simulation studies are colored green. Amino acids are colored red. Figure taken from Adebiyi et al. (2014).

^{13}C MFA to be performed based on an extensive metabolic model that included a complete TCA cycle, as recently reported by Zhang and Bryant (2011). In both cases, the addition of glycerol to the media resulted in a higher growth rate, and both groups also noted incorporation of CO_2 through anaplerotic pathways involved in the formation of oxaloacetate (OAA) from PEP (i.e., C4-like metabolism). Further evaluation of this strain would benefit from standardized growth conditions and also by extending the ^{13}C MFA studies to include additional isotopomer measurements beyond those obtained from proteinogenic amino acids.

Isotopically nonstationary ^{13}C MFA. The development of software packages, such as INCA, has enabled INST-MFA studies of autotrophic metabolism in cyanobacteria. These complement previous studies that have been limited to heterotrophic or mixotrophic conditions. The approach was first applied by Young et al. (2011) to the model cyanobacterium *Synechocystis* growing in a controlled photobioreactor. The study relied on both GC-MS and LC-MS/MS to quantify labeling trajectories of 15 intracellular metabolites following administration of ^{13}C-labeled bicarbonate to the culture. This was the first comprehensive flux analysis performed using isotope labeling data obtained in a fully autotrophic system. Steady-state labeling was typically achieved in less than 10 minutes, with the notable exception of TCA pathway intermediates (e.g., succinate, fumarate, and citrate) that were more slowly labeled. The flux map obtained using ^{13}C INST-MFA was compared to a previously published linear programming solution that predicted the theoretical optimum flux profile needed to maximize growth and minimize light utilization (Shastri and Morgan 2005). Overall, the results indicated that photoautotrophically grown *Synechocystis* cells exhibited suboptimal carbon efficiency, with significant loss of fixed CO_2 via oxPPP. This provides an example of how flux analysis can be used to identify pathways responsible for reduced productivity, by pinpointing processes that

contribute to carbon losses. These pathways offer potential metabolic engineering targets that can be manipulated to increase flux to desirable products.

Earlier that same year, Huege et al. (2011) published results from a transient ^{13}C labeling study comparing wild-type *Synechocystis* and two photorespiratory pathway mutants pre-acclimated to either high carbon (HC) or low carbon (LC) conditions. In the absence of a comprehensive flux analysis, metabolite turnover rates were assessed to provide local flux estimates (e.g., sucrose production) based on the observed dynamics of total ^{13}C enrichment. Despite differing growth and labeling conditions, the wild-type results were largely in agreement with the findings of Young et al. (2011). It was determined in both cases that activity of C3 metabolism involving RuBisCO was the primary source of carbon fixation, although C4 metabolism through PEP carboxylase (PEPC) was active to a lesser degree as noted in the *Cyanothece* studies (Feng et al. 2010; Alagesan et al. 2013). However, Huege et al. noted PEPC activity only in LC conditions, whereas Young et al. calculated flux in the equivalent of HC conditions. Both groups noted that RuBisCO oxygenase activity was very low in the wild-type strains. Also, the glyoxylate shunt was found to be inactive in both of these studies, as no evidence was found in the ^{13}C labeling data to support its presence under photoautotrophic conditions. Lastly, both groups noted the possibility of metabolite channeling within pathways, where enzymes catalyzing successive reactions cluster together spatially in order to minimize diffusional limitations. This effect was revealed by more rapid ^{13}C enrichment and higher steady-state labeling of some downstream metabolites relative to upstream metabolites, which could not be explained in the absence of metabolite channeling.

A similar transient ^{13}C labeling study was recently combined with intracellular metabolite profiling to investigate cellular response to nitrate depletion in cyanobacteria (Hasunuma et al.

2013). In *Arthrospira platensis* and *Synechocystis*, the rate of ^{13}C incorporation in central carbon metabolites and amino acids was determined over a thirty-minute labeling period using $NaH^{13}CO_3$. In comparison with cells grown under nitrogen-replete conditions, nitrogen depletion resulted in lower cell growth rate, lower percentage of proteins in the cell, and higher glycogen content. The ^{13}C labeling data indicated that, with the exception of glutamine and glutamate, the enrichment of most intracellular metabolites was significantly decreased in *A. platensis* cells cultivated without nitrate. These findings suggest that cyanobacteria placed under nitrogen stress conditions degrade intracellular proteins to amino acids, which then serve as the carbon source for glycogen synthesis.

Summary. MFA has proven useful for elucidating pathways in cyanobacteria. Both SS- and INST-MFA have been used to increase understanding of central carbon metabolism, particularly the use of oxPPP versus CBB and minimal activity in the TCA cycle and photorespiration. Different feed and light conditions exhibited shifts in metabolism to ensure continuous production of NADPH in the presence and absence of light. OxPPP was the prominent pathway in heterotrophic cells but was also found to be active in mixotrophic cells and even photoautotrophic cells, indicating decreased efficiency in carbon metabolism. Conversely, CBB flux was prominent in photoautotrophic cells and higher than glucose flux in mixotrophic cells. Combining MFA with other analysis methods provided deeper understanding of regulation and specifically demonstrated the uncoupling of transcription and translation with metabolism. Overall, this information can be used to identify interesting pathways for introducing biofuel or biochemical synthesis genes by highlighting sources of abundant carbon versus unused pathways.

Optimization of Pyruvate-derived Products in Cyanobacteria

Pyruvate is produced as the end point of glycolysis and serves as a key metabolic node for downstream branches of metabolism, including amino acid synthesis and the TCA cycle (Figure 2.3). In metabolic engineering, this metabolite also serves as a precursor for a number of products of interest. This review briefly focuses on cyanobacterial production of two of these products and the metabolic engineering approaches used to increase productivity in two platform strains, *Synechocystis* sp. PCC 6803 and *Synechococcus elongatus* sp. PCC 7942.

Cyanobacterial production of ethanol. Ethanol is one of the most visible biofuels in use today. Current production in the U.S. is primarily achieved by processing starch-based crops, such as corn. Recent legislation seeks to increase the volume of ethanol produced, but this adds excess agricultural stress by requiring increases in crop yields and also in land use (Khoo 2015). Research has gone into production of ethanol from platform microbes, such as *Escherichia coli*. Toxicity is a primary limitation to large-scale production. Also, these microbes still require some high cost carbon source, negating some of their benefits. Photoautotrophic cyanobacteria remain superior in this regard, but productivity remains a significant drawback.

Exploration into ethanol production by cyanobacteria began in the strain *Synechococcus elongatus* sp. PCC 7942 (*S. elongatus*). This strain was engineered by Deng and Coleman (1999) through addition of pyruvate decarboxylase (*pdc*) and alcohol dehydrogenase II (*adh*) from *Zymomonas mobilis* (Figure 2.3). Genes were first placed under control of the ribulose 1,5-bisphosphate carboxylase/oxygenase large and small subunit (*rbcLS*) promoter. The promoter led to high expression of PDC and ADH and resulted in ethanol production of 63 mg L^{-1} over 21 days (3 mg L^{-1} day^{-1}) in liquid batch cultures. Further, the *pdc* start sequence and ribosome binding site were replaced with the start sequence and ribosome binding site of *rbcLS*.

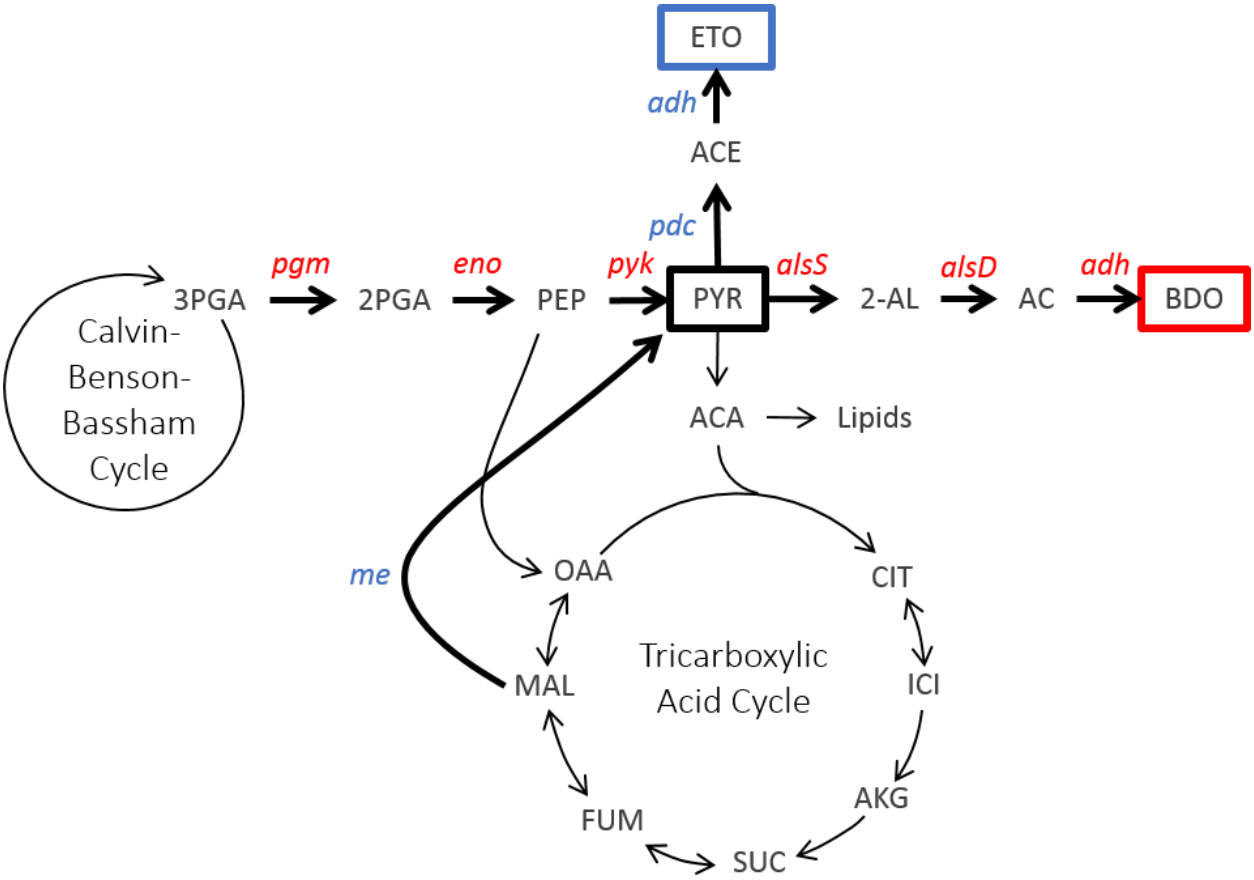

Figure 2.3 – Biosynthetic metabolism of cyanobacteria. Highlighted are the pathways introduced or engineered for production of pyruvate derivatives, ethanol (blue) and 2,3-butanediol (red). Abbreviations: **2-AL:** 2-acetolactate; **2PGA**: 2-phosphoglycerate; **3PGA**: 3-phosphoglycerate; **AC**: acetoin; **ACA:** acetyl-CoA; **ACE**: acetaldehyde; ***adh***: alcohol dehydrogenase; **AKG:** α-ketoglutarate; ***alsD***: acetolactate decarboxylase; ***alsS***: acetolactate synthase; **BDO**: 2,3-butanediol; **CIT:** citrate; ***eno***: enolase; **ETO**: ethanol; **FUM**: fumarate; **ICI**: isocitrate; **MAL**: malate; ***me***: malic enzyme; **OAA**: oxaloacetate; ***pdc***: pyruvate decarboxylase; **PEP**: phosphoenolpyruvate; ***pgm***: phosphoglycerate mutase; ***pyk***: pyruvate kinase; **PYR**: pyruvate; **SUC**: succinate.

This modification led to a 2-fold increase in *pdc* expression and an increase in ethanol production to 79 mg L^{-1} (3.8 mg L^{-1} day^{-1}). Based on the experimental set up, these values were estimated as having a 5 – 15% loss. However, these values remained 100-fold less than the theoretical yield based on *in vitro* enzyme activity assays, which yielded 160 nmol min^{-1} mg of total $protein^{-1}$, corresponding to a theoretical synthesis rate of 276 mg ethanol OD_{730}^{-1} L^{-1} day^{-1} versus 2.5 mg ethanol OD_{730}^{-1} L^{-1} day^{-1} produced in an aerated culture. This resulted in the conclusion that there was some limitation other than PDC and ADH activity.

The next exploration into cyanobacteria-produced ethanol was in *Synechocystis* sp. PCC 6803 (*Synechocystis*) (Dexter and Fu 2009), the first cyanobacterium with a fully-sequenced genome. Again, *pdc* and *adh* were cloned from *Z. mobilis*. The genes were placed under control of the light-driven photosystem II (*psbAII*) promoter. Production reached 230 mg L^{-1} in 5 days (average 46 mg L^{-1} day^{-1}) when grown in batch and around 553 mg L^{-1} in 6.5 days (average 85 mg L^{-1} day^{-1}) when grown in a photobioreactor. After some time, though, a steep decline in ethanol concentration was observed, highlighting the reversibility of the *adh* enzyme. At its peak, the ethanol concentration remained within the range at which toxicity was determined to have minimal impacts on cell growth (about 10.6 g L^{-1}). Therefore, the observed reduction in growth was attributed to metabolic reprogramming.

Gao et al. (2012) also focused on ethanol production by *Synechocystis*. The genes were placed under control of the RuBisCO promoter, as with Deng et al. Production was optimized by introducing two copies of *pdc* from *Z. mobilis* and overexpressing endogenous *adh* rather than introducing the gene from an exogenous source. The genes were integrated into a neutral site and into the position of the poly-β-hydroxybutyrate (PHB) producing gene to decrease pyruvate lost to PHB simultaneously. This strain yielded 5.50 g L^{-1} over 26 days in a photobioreactor

(average 212 mg L^{-1} day^{-1}), an increase over strains engineered with *pdc* and *adh* both from *Z. mobilis* (1.12 g L^{-1} or 43 mg L^{-1} day^{-1}).

A recent investigation tested the effect of malic enzyme (ME), a pyruvate-forming enzyme, on ethanol production in *Synechocystis* (Yoshikawa et al. 2015). ME was initially deleted. *Pdc* and *adh* from *Z. mobilis* were then added to this strain as well as the wild-type strain. Genes were placed under control of the promoter for *nblA*, a key protein of phycobilisomes degradation, because promoters from both *psbA2* and *rbcLS* led to severe growth inhibition. Knocking out ME led to a decrease in flask production of ethanol compared to the wild-type, 379 ± 10 mg L^{-1} versus 422 ± 9 mg L^{-1} over 12 days (31.6 mg L^{-1} day^{-1} versus 35.2 mg L^{-1} day^{-1}). ME was reconstituted in the knockout strain and overexpressed in the wild-type strain under control of the *psbA2* promoter. This led to an 18-fold increase in ME expression and over 2-fold decrease in malate intracellular concentration compared to the wild-type ethanol producing strain. However, maximal production only increased to 431 ± 19 mg L^{-1} (35.9 mg L^{-1} day^{-1}). The authors suggested that ME expression was likely outside of the range optimal for ethanol production due to the strength of the promoter.

Despite the increases in productivity, these strains still yielded far less than industry standard. A recent review on ethanol production by cyanobacteria discusses industrial production by companies such as Algenol Biofuels and Joule Unlimited (Dexter and Fu 2009). The highest reported productivity is 552 mg L^{-1} after 1 day by Algenol (Piven et al. 2014). Of the academic research efforts, the highest reported productivity of 212 mg L^{-1} day^{-1} was achieved using a strong native promoter and the native *adh* (Gao et al. 2012). The most notable difference between this approach and others mentioned was the successful elimination of a competing PHB synthesis, leading to increased flux from pyruvate to the desired pathway and increasing production almost

5-fold. Moving forward, methods of eliminating competing pathways should be further investigated to increase carbon to pyruvate and, further, to ethanol.

Cyanobacterial production of 2,3-butanediol. The alcohol 2,3-butanediol (BDO) is another pyruvate derivative. Like ethanol, BDO has potential as a drop-in fuel (Savakis et al. 2013). It is currently in use as the precursor for methyl ethyl ketone, 2-butanol, and 1,3-butadiene, which is used to produce polymer and copolymer materials.

The pathway for biological synthesis of BDO begins at the pyruvate node (Figure 2.3). Acetolactate synthase (ALS or *alsS*) converts pyruvate to 2-acetolactate (2AL). Next, acetolactate decarboxylase (ALDC or *alsD*) converts 2AL to acetoin. This intermediate is more acutely toxic to cells, as will be shown later, and may also be secreted and taken up by the cells. The final step in BDO synthesis involves acetoin reductase, a secondary alcohol dehydrogenase (AR or *adh*), which converts acetoin to BDO.

Within the cells, ALDC yields *(R)*-acetoin, which may be converted either to *(meso)*-BDO or *(R,R)*-BDO, depending on the reducing enzyme. If the acetoin is secreted, high pH in the supernatant may result in its racemization to *(S)*-acetoin, yielding *(S,S)*-BDO when taken up by the cells and dehydrogenated by AR. These factors have been taken into account in the optimization steps performed by the two groups who have studied BDO synthesis in cyanobacteria.

The first strain of cyanobacteria used for production of BDO was *Synechocystis* (Savakis et al. 2013). Toxicity for this strain was measured as IC50 values of 375 mM (33.8 g L^{-1}) for BDO and 95 mM (8.4 g L^{-1}) for acetoin. The first set of enzymes tested were ALS from *Enterococcus faecalis*, ALDC and AR from *Lactococcus lactis* sp. *cremoris*. A catabolic ALS was chosen rather than an anabolic analog to avoid feedback inhibition from branched chain amino acids. The genes were introduced individually under control of the promoter Pt5 for low, unregulated expression

and yielded a 12-day production of 2.2 mg L^{-1} of acetoin (0.18 mg L^{-1} day^{-1}) and 10.9 mg L^{-1} of BDO (0.91 mg L^{-1} day^{-1}). A second set of enzymes were introduced into a new strain as a single operon under control of IPTG-inducible P_{trc} promoter. Using ALS from *Leuconostoc lactis* NCW1, ALDC from *Bacillus brevis*, and AR from *Enterobacter* sp. 638 led to acetoin production of 18.5 mg L^{-1} and a mixture of 20.0 mg L^{-1} and 9.0 mg L^{-1} of *(meso)*- and D/L-BDO, respectively over 12 days (1.5 mg L^{-1} day^{-1} of acetoin and 2.4 mg L^{-1} day^{-1} total BDO). A subsequent *in vitro* characterization of ALS from *L. lactis* NCW1 revealed low activity of the enzyme, hinting that *Synechocystis* had its own active ALS. Deleting the exogenous ALS from this strain led to an increase in regulation of the remaining proteins ALDC and AR over 2.5- and 1.5-fold, respectively. The culture medium was also modified by removing the excess bicarbonate because its addition was found to downregulate native ALS. Under these conditions, acetoin and BDO production reached 120 mg L^{-1} and 590 mg L^{-1} over 29 days with an average daily production around 5.8 mg L^{-1} day^{-1} and 9.0 mg L^{-1} day^{-1}. Finally, cofactor balances were optimized to control the BDO-to-acetoin ratio. Addition of a soluble transhydrogenase (*sth*; $NADPH + NAD^+ \leftrightarrow NADP^+ + NADH$) from *Pseudomonas aeruginosa* decreased acetoin as a secreted product to around 20 mg L^{-1} over 13 days (1.5 mg L^{-1} day^{-1}) and increased BDO to 140 mg L^{-1} over the same time period (11 mg L^{-1} day^{-1}). Enzymatically, the AR from *Enterobacter* was replaced with an NADPH-dependent AR from *L. lactis* NCW1 to take advantage of high NADPH levels under photosynthesis. Levels of acetoin and the racemic product *(S,S)*-BDO resulting from acetoin in the supernatant remained undetectable over 13 days while levels of *(meso)*-BDO peaked at 190 mg L^{-1} (15 mg L^{-1} day^{-1}).

At the same time Savakis et al. were studying BDO production in *Synechocystis*, Oliver et al. (2013) were applying similar efforts to *S. elongatus*. As with *Synechocystis*, toxicity was

measured first, but *S. elongatus* was found to be more acutely sensitive to the products. Acetoin led to a 42% decrease in growth in the first 24 hours at a concentration of 0.2 g L^{-1} versus an IC50 of 8.4 g L^{-1} in *Synechocystis*. The cells were less sensitive to BDO than acetoin, though, exhibiting a 2.2% and 8.9% decrease in growth at concentrations of 10 g L^{-1} and 30 g L^{-1}, respectively.

Engineering began with introduction of the ALS gene from *Bacillus subtilis* under control of the IPTG-inducible promoter, $P_L lacO_1$. Various ALDC enzymes were tested, and two were chosen for further investigation. ALDC from *Enterobacter aerogenes* resulted in moderate acetoin production of 108 mg L^{-1} over 72 hours (36 mg L^{-1} day^{-1}), while ALDC from *Aeromonas hydrophila* yielded high acetoin levels, 203 mg L^{-1} over 72 hours (68 mg L^{-1} day^{-1}). A similar screening was performed to select the final enzyme in the pathway, referred to as secondary alcohol dehydrogenase (ADH). Four enzymes were chosen, two producing BDO in the *(R)*-configuration and two producing the *(S)*-configuration. Of these four, the highest productivity in the moderate strain over 72 hours was achieved using ADH from *Thermoanaerobacter brockii*, which yielded 301 mg L^{-1} BDO (100 mg L^{-1} day^{-1}) with 50 mg L^{-1} of acetoin (17 mg L^{-1} day^{-1}). However, ADH from *Clostridium beijernickii* yielded the highest productivity with *A. hydrophila* ALDC, 952 mg L^{-1} BDO (320 mg L^{-1} day^{-1}) with 61 mg L^{-1} acetoin (20 mg L^{-1} day^{-1}) compared to 568 mg L^{-1} (190 mg L^{-1} day^{-1}) with 59 mg L^{-1} acetoin (20 mg L^{-1} day^{-1}) produced using ADH from *T. brockii*. Long term 21-day culturing of these two strains yielded 2.38 g L^{-1} BDO with *C. beijernickii* ADH and 1.97 g L^{-1} with *T. brockii* ADH (790 mg L^{-1} day^{-1} and 660 mg L^{-1} day^{-1}, respectively). When *lacI* was transcribed in these strains as a repressor, constitutive expression was observed in the absence of the inducer IPTG, indicating the presence of leaky expression within the construct. It was also observed that increasing enzyme expression did not lead to

increased product formation, suggesting a substrate limitation, likely of pyruvate. These two factors have been addressed in the next two papers.

The first limitation addressed was that of pyruvate availability. Because metabolites from the Calvin-Benson-Bassham (CBB) cycle are necessary for carbon fixation, much of the carbon in central carbon metabolism is cycled within this pathway rather proceeding from 3-phosphoglycerate (3PGA) towards pyruvate (Figure 2.3) (Oliver and Atsumi 2015). This work targeted the 3PGA to pyruvate pathway within the background of a previously optimized strain containing *alsS* from *B. subtilis*, *alsD* from *A. hydrophila*, and *adh* from *C. beijernickii*. Overexpressing the first enzyme phosphoglycerate mutase (*pgm*) in this pathway had no significant effect, but overexpressing the final pyruvate kinase (*pyk*) led to a significant growth defect. Total BDO production by these cells remained similar to the control strains, leading to an increased per-cell productivity and a final titer around 20 mg L^{-1} for one strain (strain 9) after 96 hours (5 mg L^{-1} day^{-1}). Overexpression of all three genes between 3PGA and pyruvate led to slower growth compared to the control but also to a final titer up to 49 mg L^{-1} (12 mg L^{-1} day^{-1}) over 96 hours. Increasing the light intensity from 55 to 250 μmol photons m^{-2} s^{-1} and increasing the starting culture density led to a peak production of 726 mg L^{-1} over 60 hours (290 mg L^{-1} day^{-1}) by strain 9 versus 535 mg L^{-1} produced by the control strain (214 mg L^{-1} day^{-1}). Production by the *pyk* overexpressing strain also increased to 500 mg L^{-1} over 60 hours (200 mg L^{-1} day^{-1}), and growth increased as well. Overexpression of the enzymes within the 3PGA to pyruvate pathway under high light and high cell density conditions led to an almost 1.4-fold increase in BDO productivity.

Nozzi et al. (2015) addressed the issue of leaky expression by using a superfolder green fluorescent protein (sfGFP) as a reporter. After eliminating the promoter $P_L lacO_1$ as a source, leaky

expression was discovered in *alsS* and *adh* but not *alsD*. A bacterial promoter prediction program identified four and three potential promoter sites, respectively, but testing each site showed the leaky expression was a cumulative effect. The greatest constitutive promoter effect was detected in *alsS*. ADH activity increased when placed directly downstream of this gene. Rearranging the enzyme order from *alsS-alsD-adh* to *alsD-alsS-adh* successfully suppressed expression in the absence of IPTG. This led to lower productivity (45 mg L^{-1} OD_{730}^{-1} versus 125 mg L^{-1} OD_{730}^{-1} with addition of 1 mM IPTG). However, this was because the leaky expression led to higher accumulation of BDO before IPTG addition in the base strain. This final article highlighted sources of leaky expression in exogenous or overexpressed genes and illustrated the tightness in control that may be achieved by modifying gene order.

The 2,3-butanediol synthesis pathway has been successfully introduced into cyanobacteria. These analyses highlight a primary difference between two commonly-used strains, *Synechocystis* and *S. elongatus*, that is, that the former exhibits higher tolerance to potentially toxic products (Kämäräinen et al. 2012). Metabolic engineering platform decisions should consider this factor. The highest productivity was observed in *S. elongatus*, peaking at 790 mg L^{-1} day^{-1} in a 21-day production experiment (Oliver et al. 2013). Subsequent optimization resulted in further improvement of this strain by increasing pyruvate through overexpression of enzymes within the pathway from 3PGA to pyruvate. The productivity of the control in this experiment was lower than the reported values in the previous paper, suggesting culture differences. However, the enzyme overexpressing strain showed almost a 1.4-fold increase over the control strain under the same conditions. The final optimization scheme of eliminating leaky expression is an especially beneficial consideration in systems for which product formation involves growth-inhibiting steps, for example, with the pyruvate kinase overexpression. By maintaining this control, cultures can be

grown to higher cell densities before product formation is induced, decoupling the two carbon sinks and increasing carbon available for product synthesis.

Summary. Production of these two pyruvate derivatives show promise in increasing the industrial feasibility of cyanobacteria. The primary benefit of cyanobacteria over more rapidly growing bacteria is its ability to fix CO_2. More recently, a group introduced CO_2-fixing mechanisms within the heterotrophic *E. coli* (Gong et al. 2015). However, the fixed carbon accounted for less than 20% of carbon entering central carbon metabolism, representing mixotrophic growth, which is already feasible in many strains of cyanobacteria, including *Synechocystis*. The engineering approaches successfully applied within the optimized strains presented within this literature review include the following:

1) engineering genes, including promoter and ribosome binding site optimization, gene codon optimization, and gene order optimization,
2) eliminating pathways competing for the pyruvate, specifically PHB synthesis,
3) optimizing enzymes introduced, either by screening exogenous genes or by evaluating the potential of endogenous genes, and
4) adjusting culture conditions, from altering media additives to fit the genes of interest to increasing cell density to account for low growth/high product strains.

These steps consistently yielded increases in product formation and provide avenues for increasing the productivity of cyanobacteria.

CHAPTER III

SIMULATION STUDY OF METABOLIC FLUX ANALYSIS

Introduction

Metabolic flux analysis (MFA) is a mathematical modeling approach used to determine flow of material through intracellular biochemical pathways comprehensively (Nielsen 2003; Sauer 2006; Stephanopoulos 1999; Wiechert 2001). The final outcome of MFA is a flux map that depicts the *in vivo* activity of metabolic enzymes. This information can be used (i) to identify major intracellular pathways and critical branch points in the metabolic network, (ii) to calculate rates of otherwise unmeasurable pathways, and (iii) to determine maximum theoretical yields for synthesis of products or biomass from complex, integrated biochemical pathways (Woolston et al. 2013). However, MFA is most useful when flux comparisons can be made between different strains or growth conditions and also when combined with other phenotypic data sets. This enables researchers (i) to understand flux control at metabolic branch points (Vallino and Stephanopoulos 1994), (ii) to identify kinetic or regulatory bottlenecks in the metabolic network (Antoniewicz et al. 2007), and (iii) to identify targets for re-routing flux to desirable end products (or away from wasteful byproducts). One classic example that illustrates the application of MFA for rational target selection is the overproduction of lysine in the soil bacterium *Corynebacterium glutamicum*, which has been expertly summarized by Koffas and Stephanopoulos (2005).

MFA begins with translation of available biochemical and genomic information into a set of mathematical equations representing metabolite mass balances. This system of equations can be augmented by various thermodynamic and/or regulatory constraints. Stoichiometric MFA

approaches apply these balance equations to solve for intracellular fluxes based on measurements of extracellular substrate consumption or product formation rates. However, the system of mass balance equations is typically underdetermined for realistic metabolic networks, and therefore, it is not possible to solve for all intracellular fluxes without making additional *ad hoc* assumptions. In this case, optimization-based or constraint-based methods are often applied to explore the space of possible solutions, rather than attempting to identify a unique flux solution. Alternatively, additional measurements derived from isotope labeling experiments (ILEs) can be used to generate an overdetermined system of equations that can be solved using least-squares regression. ILE are accomplished using substrates with isotopically labeled atoms, typically carbon-13 (^{13}C) or deuterium (^{2}H). This allows the metabolic model to be expanded to include mass isotope isomer (isotopomer) balances of individual metabolites in addition to overall mass balances, altogether providing the mathematical basis for ^{13}C MFA calculations.

Two different ^{13}C MFA approaches have been applied to cyanobacteria: steady-state MFA (SS-MFA) and isotopically nonstationary MFA (INST-MFA) (Figure 2.1). A brief review of these applications is found in Chapter 2. The term "steady-state" refers to isotopic steady state, in which labeling measurements are obtained after ^{13}C from introduced substrates has fully incorporated into intracellular metabolites. Ideally, the experiment is performed in a continuous culture to maintain metabolic steady state throughout the ILE. Alternatively, cells growing exponentially (rapidly dividing) in batch culture may be used to approximate metabolic steady state conditions. The isotope tracer for SS-MFA is typically a mixture of ^{13}C-labeled glucose analogs, the composition of which is selected to maximize flux precision within the pathways of interest (Antoniewicz 2013). Under these conditions, cyanobacteria exhibit mixotrophic or heterotrophic metabolism. INST-MFA becomes necessary for studies of autotrophic metabolism. In autotrophic

cultures, the condition of isotopic steady state is no longer ideal because addition of single carbon tracers ($^{13}CO_2$ or $NaH^{13}CO_3$) results in a uniform ^{13}C-labeling pattern in the downstream metabolites. These steady-state labeling measurements fail to reflect carbon atom rearrangements within the network (Shastri and Morgan 2007). Rather, transient measurements of isotope incorporation following a feed switch from natural $H^{12}CO_3^-$ to enriched $H^{13}CO_3^-$ are used to estimate autotrophic fluxes in INST-MFA (Young et al. 2011).

Recently, a package of MATLAB routines, called INCA (Isotopomer Network Compartmental Analysis), was developed to automate the computational workflow of INST-MFA (Young 2014). This program solves the coupled system of ordinary differential equations that comprise the transient isotopomer balances. INCA relies on the elementary metabolite unit framework to simulate transient ^{13}C labeling experiments efficiently (Young et al. 2008), allowing for application of INST-MFA to metabolic networks of arbitrary size and complexity. As with SS-MFA, the biological system must be maintained at metabolic steady state throughout the labeling time course, but INST-MFA tracer experiments are performed on a time scale of minutes rather than hours to assess the dynamics of ^{13}C incorporation (Nöh and Wiechert 2006). Rapid sampling and cold-quenching of cells are required to arrest the *in vivo* labeling state of central carbon metabolites, which is then measured in cell extract samples using mass spectrometry (Jazmin et al. 2014; Jazmin and Young 2013).

In INST-MFA, a stable isotopically labeled carbon source is introduced to cells, and the labeling of the intracellular metabolites is measured over a series of time points (Figure 3.1). Gas chromatography with mass spectrometry (GC/MS) is used to quantify the mass isotopomer distribution of each metabolite at each time point. This yields a large amount of data. To aid in simplifying this method of analysis, a previous model was probed to assess if there exists a minimal

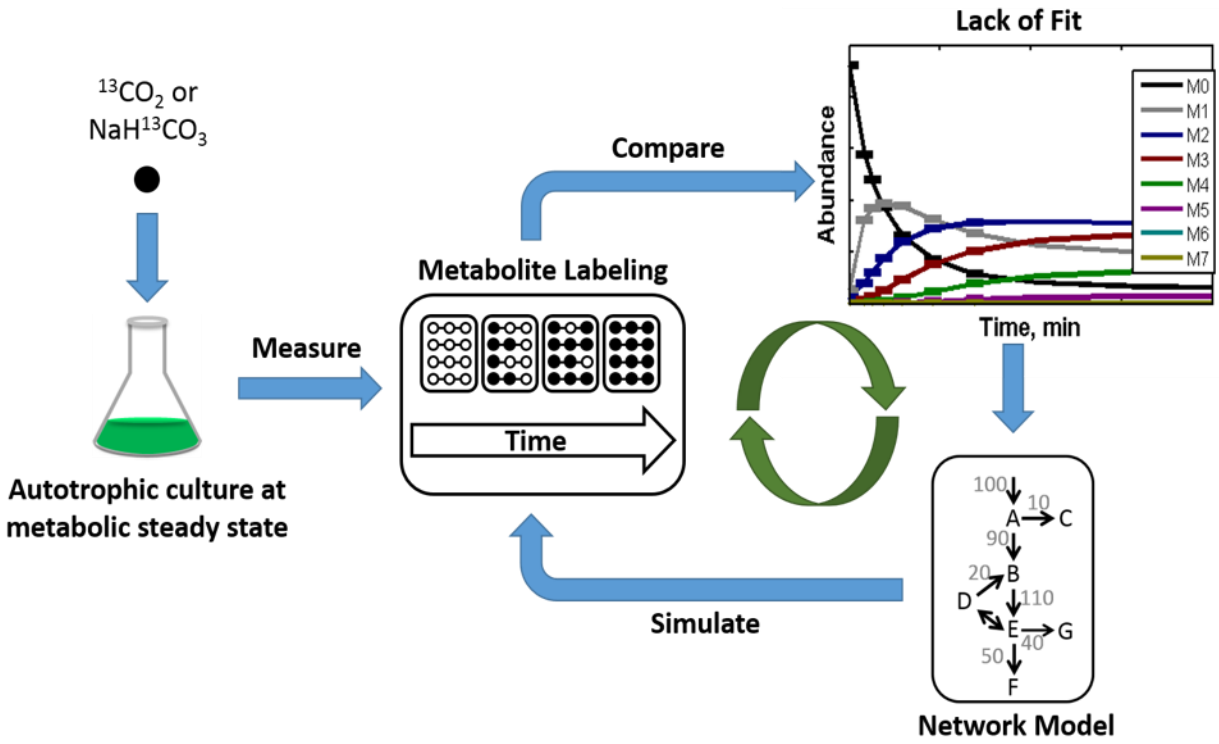

Figure 3.1 – Workflow of INST-MFA in cyanobacteria. Labeled CO_2 or bicarbonate is fed to a culture at metabolic (quasi)steady state, and metabolite labeling is measured over time using mass spectrometry. The mass isotopomer distributions (MIDs) of all measured metabolites are compared with simulated values produced by a mathematical model of the transient isotopomer balances. The fluxes in the model are iteratively adjusted until the simulated MIDs match their experimentally determined values. Figure taken from Adebiyi et al. (2014).

set of data that could be inputted into INCA and yield a reliable set of flux estimates. The following sections provide data on subsets of metabolite and time points, emphasizing which groupings most affected flux uncertainties and highlighting their significance within the metabolic model.

Method

The precision of flux estimates obtained from INST-MFA is dependent upon the measurement of metabolite labeling within the pathways of interest. In order to assess the relative importance of the measurements included in a prior cyanobacteria study (Young et al. 2011), the same model and flux estimates were used to simulate time-course mass isotopomer measurements at the times listed in Table 3.1. Then best-fit model parameters were estimated using the full complement of MS measurements and assuming 0.5 mol% uncertainties on all values (Base Case model). Next, all of the mass isotopomer measurements used for the simulation were separated into one of six groups based on their location within the metabolic network (Table 3.2 and Figure 2.2) and the fluxes were re-estimated after inactivating each group, separately. Inactivating measurements did not change the best-fit values of the estimated fluxes, but the estimated uncertainties fluctuated in several cases.

To precisely quantify flux uncertainties, 95% confidence intervals (CIs), indicating the range of feasible flux values given the available data, were computed for the following six net fluxes, which together span the null space of the stoichiometric matrix and represent all independent degrees of freedom for the model: glucose-6-phosphate (G6P) dehydrogenase (G6PDH), part of the oxidative pentose phosphate pathway (oxPPP); ribulose-1,5-bisphosphate (RUBP) carboxylase (RBC) and sedoheptulose-1,7-bisphophatase (SBPase), both from the Calvin-Benson-Bassham (CBB) cycle; RUBP oxygenase (RBCOX) of the photorespiratory (PR)

Table 3.1 – Simulated time points for mass isotopomer measurements.

	time (s)	
	calculated	adjusted
0	0	0
1	20.0	20
2	30.5	30
3	46.6	45
4	71.1	70
5	108.6	110
6	165.8	165
7	253.0	250
8	386.2	390
9	589.6	590
10	900.0	900

Time points are calculated as suggested by Nöh and Wiechert (2006) using $t_i = ab^{i-1}$ for $a = 20$ and $b = 1.525$. Exact times were rounded as shown. Table taken from Adebiyi et al. (2014).

Table 3.2 – Ion fragment groupings by pathway.

CBB-3C/6C (G1)	CBB-5C/7C (G2)	TCA (G3)	PEP-cyc (G4)	PR (G5)	oxPPP (G6)
3PGA185 (1.1)	R5P229 (2.1)	SUC247 (3.1)	PEP167 (4.1)	GA292	G6P259
3PGA357 (1.1)	RUBP309 (2.2)	FUM245 (3.2)	MAL233 (4.2)	GA307	
3PGA459 (1.1)	S7P289 (2.3)	CIT273 (3.3)			
DHAP169 (1.2)	RU5P229 (2.4)	CIT363 (3.3)			
F6P259 (1.3)		CIT375 (3.3)			
GAP169 (1.4)		CIT465 (3.3)			

The mass spectrometry metabolite ion fragments from the original INST-MFA model (Young et al. 2011) were placed into groups based on pathway and size. Pathways include Calvin-Benson-Bassham cycle, tricarboxylic acid (TCA) cycle, PEP-MAL cycle, photorespiration, and the oxidative pentose phosphate pathway. Abbreviations: **3PGA**: 3-phosphoglycerate; **CIT**: citrate; **DHAP**: dihydroxyacetone phosphate; **F6P**: fructose-6-phosphate; **FUM**: fumarate; **G6P**: glucose-6-phosphate; **GA**: glycerate; **GAP**: glyceraldehyde-3-phosphate; **MAL**: malate; **PEP**: phosphoenolpyruvate; **R5P**: ribose-5-phosphate; **RUBP**: ribulose-1,5-bisphosphate; **RU5P**: ribulose-5-phosphate; **S7P**: sedoheptulose-7-phosphate; **SUC**: succinate. Table taken from Adebiyi et al. (2014).

pathway; malic enzyme (ME) of the phosphoenolpyruvate (PEP) cycle (PEP-cyc: formed by PEP carboxylase, malate dehydrogenase, and malic enzyme); and malate synthase (MS) of the tricarboxylic acid cycle glyoxylate shunt. A group of metabolites was considered to contribute significantly to the flux uncertainty if the value increased over an arbitrary threshold of 1.5-fold in response to inactivation of the metabolites. Any groups found to be significant based on this criterion were further examined by inactivating each individual metabolite within the group to determine which contributed the most towards the observed increase in flux uncertainty.

Results and Discussion

The simulation illustrated the importance of local intermediate metabolites on flux measurements. The results from the flux uncertainty analysis fell into natural groupings based on pathway location as shown in Figure 3.2. The uncertainties of upper glycolytic enzymes G6PDH, RBC, and RBCOX increased by 1.5- to 1.6-fold upon deactivation of the CBB-5C/7C group, yet further analysis showed that this was a cumulative effect of all four metabolites within the group rather than the result of one specific metabolite. Conversely, the uncertainties of G6PDH and RBC nearly doubled with inactivation of G6P, and that of RBCOX quadrupled following inactivation of PR pathway metabolite glycerate (GA). The uncertainty of the remaining upper glycolytic flux, SBP, was strongly affected by inactivation of both CBB cycle groups. In this case, the change induced by deactivating the CBB-3C/6C group was most influenced by DHAP (1.6-fold increase), while the response to deactivating the CBB-5C/7C group was more clearly due to inactivation of the S7P measurement (8-fold increase). The final flux grouping contained enzymes ME and MS for which significant changes were observed upon inactivation of the TCA pathway measurements (over 5-fold and 2-fold, respectively) and PEP cycle measurements (over 2.5-fold and 1.5-fold,

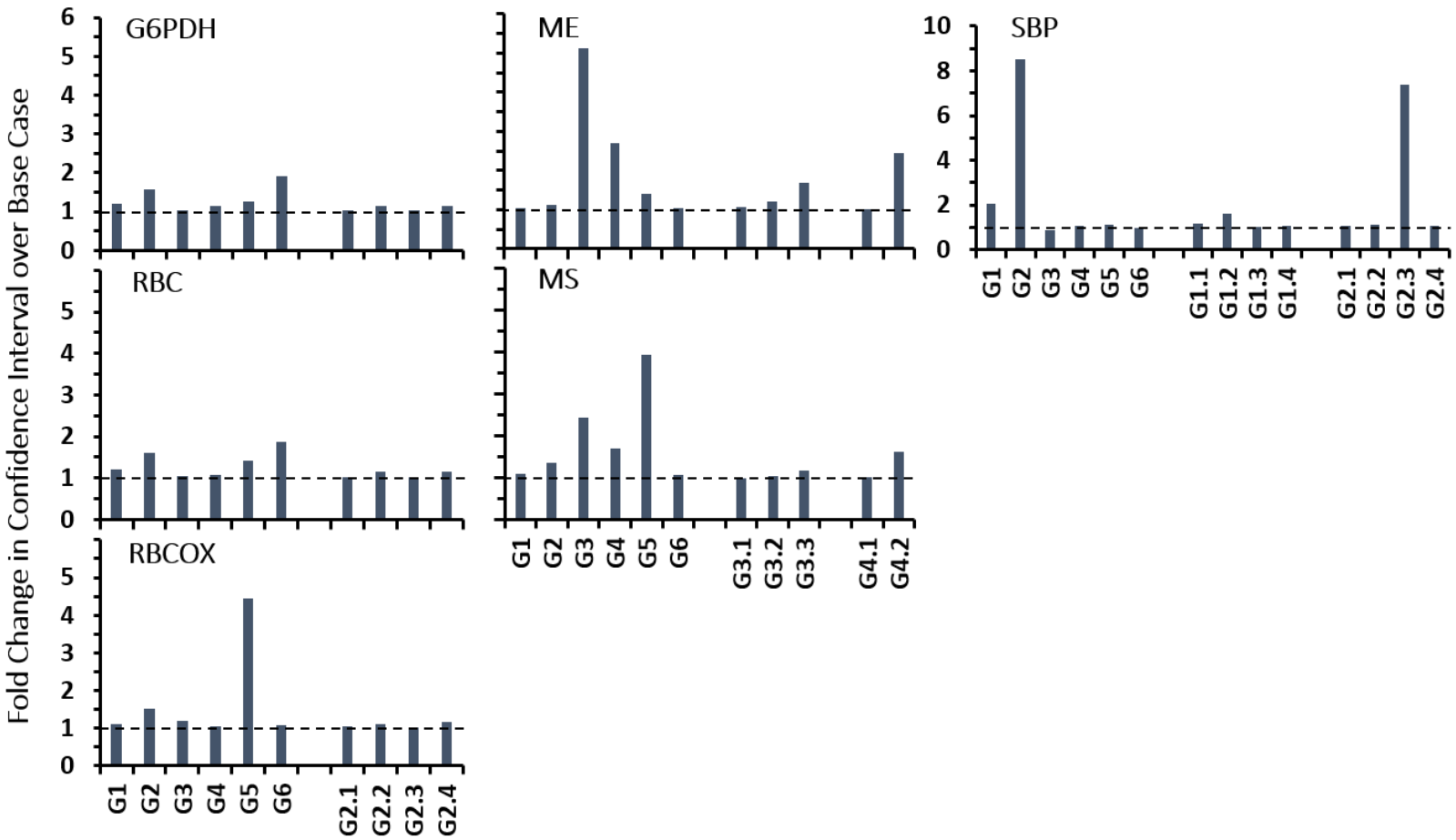

Figure 3.2 – Effect of removing measurements on flux uncertainties. Groups of measurements (G1–G6) were inactivated in the model, and the 95% confidence interval (CI) width for each of six independent fluxes was recalculated and compared to the Base Case model, which includes all measurements examined by Young et al. (2011). If the CI width increased over an arbitrary threshold of 1.5-fold, the analysis was repeated for each individual metabolite within the group to determine which one(s) contributed most to the observed increase. See Table 3.2 for a list of measurements included in each group. X-axes are aligned vertically; y-axes are aligned horizontally with the exception of SBP. Figure taken from Adebiyi et al. (2014).

respectively). Citrate contributed the most towards the importance of the TCA group, although no single measurement within this group was responsible for the entirety of the observed effect on either ME or MS. Inactivation of MAL alone led to a nearly 2.5-fold increase in the ME uncertainty and over a 1.5-fold change in the MS uncertainty. Interestingly, inactivation of GA of the PR pathway led to an almost 4-fold increase in the MS uncertainty because the MS substrate, glyoxylate, is also an intermediate of the PR pathway (Figure 2.2).

In general, each enzyme's substrate(s) and product(s) affected the flux uncertainty most significantly. Availability of these measurements directly improves the reliability of flux estimations by constraining the intermediate balance equations. Without this information, the program must estimate flux values based on less direct measurements. In cyclic pathways or reversible reactions, these metabolites become even more necessary, as seen with SBP. Furthermore, product measurements aid in estimating flux distribution between branched pathways, for example, between RBC and RBCOX. A number of metabolites across central carbon metabolism are becoming detectable using GC/MS (Wegner et al. 2014).

The effects of varying the number and span of sampling time points was also investigated. Different sets of time points were inactivated, and uncertainties were re-estimated for the same six independent fluxes (Figure 3.3). Most flux estimates were fairly robust to dropping evenly spaced time points ("Odd time points" and "Even time points"). Within this subset, only the reliability of the SBP flux estimation was affected, almost doubling upon inactivation of odd time points. This appears to be largely due to loss of information at the early time points since dropping all time points under 2 min ("Time pts 1 – 5") caused the SBP flux uncertainty to increase almost 4-fold. Conversely, the remaining fluxes were more strongly affected by inactivation of the late time points ("Time pts 6 – 10"). This is counterintuitive given that the emphasis of this method is on

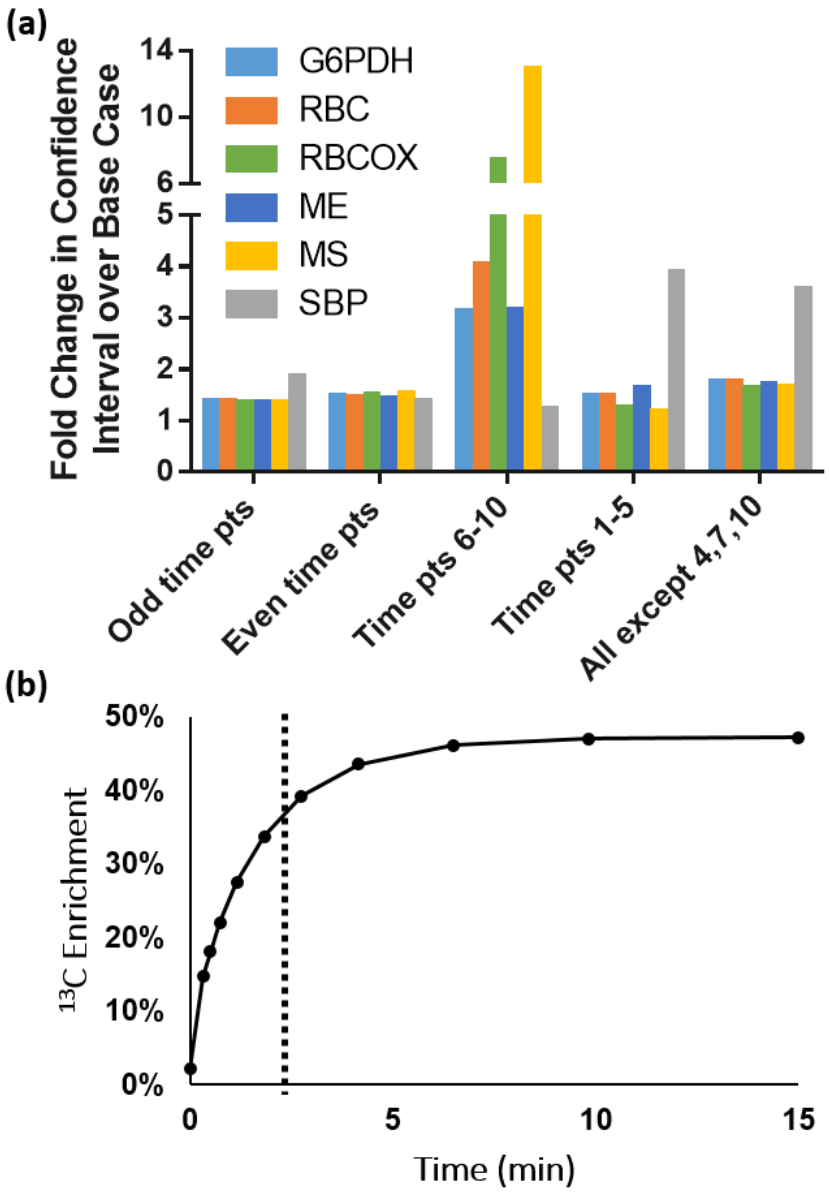

Figure 3.3 – Changes in flux uncertainties following time point inactivation. (a) Time points from Table 3.1 were inactivated in combinations as listed to determine their effect on flux uncertainty. (b) Time points are optimized to include transient ^{13}C incorporation labeling. The dotted line separates time points 1 – 5 from 6 – 10. Figure taken from Adebiyi et al. (2014).

transient incorporation of labeled carbon into intracellular metabolites. Overall, the initial time point and a small subset of the final time points are concluded to be sufficient for an initial flux estimate, though the remaining time points are still necessary to increase flux precision, as noted in comparison of "all except pts 4,7,10" to "even time points" in Figure 3.3.

Conclusion

This simulation study has provided new insights into the requirements for flux estimation using INST-MFA. The study illustrates the importance of metabolites representative of the pathways and enzymes to be observed. Specifically, the substrates and products should be included where possible, especially in cyclic or branched pathways. For time points, a reliable flux estimation may be generated using only the initial time point and three time points approaching steady-state enrichment. A select subset of the previous data has been shown as sufficient to provide an initial estimate of the six flux values using this criteria (Figure Appendix A.2). However, increasing the number of metabolites and the number of time points will aid in increasing accuracy and lowering the uncertainty of the flux estimates by increasing redundancy.

CHAPTER IV

ENGINEERING OF CYANOBACTERIA FOR INCREASED ALDEHYDE PRODUCTION

Introduction

Synechococcus elongatus sp. PCC 7942 (*S. elongatus*) has been previously engineered to produce isobutyraldehyde (IBA) (Atsumi et al. 2009) (Figure 4.1a). The gene encoding ketoisovalerate decarboxylase (KIVD) has been obtained from *Lactococcus lactis* and introduced into the *S. elongatus* genome. KIVD catalyzes conversion of the branched chain keto-acids, ketoisovalerate and ketoisocaproate, from the valine and leucine synthesis pathways into isobutyraldehyde (IBA) and isovaleraldehyde (IVA), respectively (Figure 4.1b).

IBA, the product of interest, is a direct precursor of isobutanol. As a potential fuel additive, isobutanol is an improvement over ethanol with its higher energy content (82% of gasoline versus 65%) and lower water solubility (8.5% miscible versus 100%), among other qualities (Ryan et al. 2011). This alcohol has also been used historically in place of n-butanol, primarily as a "process solvent in the flavor and fragrance, pharmaceutical, and pesticide industries" (Billig 2000). Isobutanol is produced industrially from hydrogenation of IBA, which is produced in a mixture with n-butyraldehyde (nBA) from propylene. Compared to isobutanol, the aldehyde IBA is a more advantageous target product for biosynthesis because its high volatility allows the chemical to be easily stripped from culture. This minimizes toxic effects upon the cells.

As shown in Figure 4.1a, IBA is a downstream product of pyruvate, a major metabolic node that primarily functions as the branch point between energy-producing glycolysis and the TCA cycle, which is used in most organisms to generate precursor metabolites for cell growth.

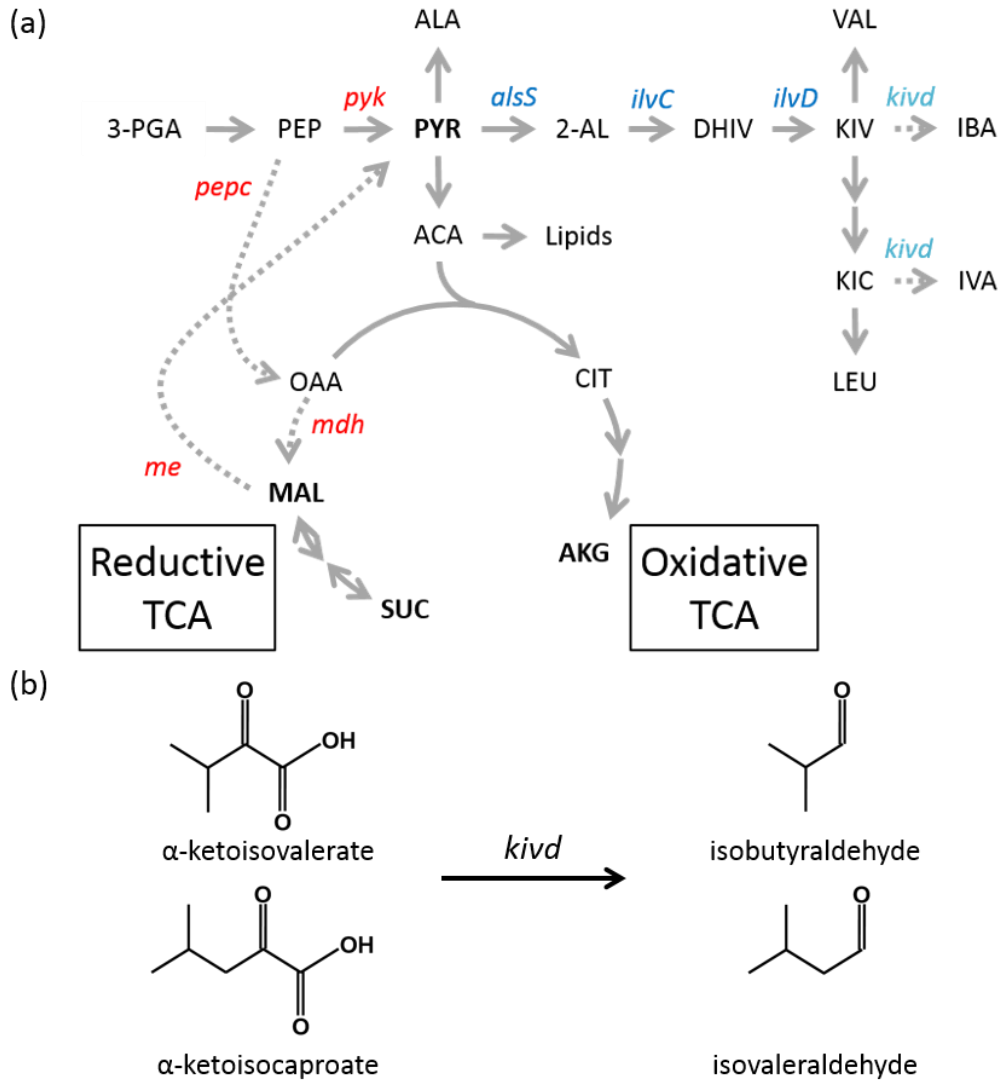

Figure 4.1 – Overview of the metabolic pathway of the IBA-producing strain. **(a)** Ketoisovalerate decarboxylase (*kivd*) from *Lactococcus lactis* was introduced into *Synechococcus elongatus* sp. PCC 7942 to convert a pyruvate derivative KIV to IBA (Atsumi et al. 2009). The strain was further optimized by addition of genes from *Bacillus subtilis* (*alsS*) and *Escherichia coli* (*ilvC* and *ilvD*). An analysis by Young et al. (2011) showed that PEP carboxylase (*pepc*), malic enzyme (*me*), and malate dehydrogenase (*mdh*) provide a natural pathway around the bottleneck in enzymatic pyruvate conversion by pyruvate kinase (*pyk*). Enzymes highlighted in blue were introduced by Atsumi et al.; enzymes in red were introduced for this project. **(b)** KIVD facilitates decarboxylation of KIV and KIC to IBA and IVA, respectively. Abbreviations: **2-AL:** 2-acetolactate; **3-PGA**: 3-phosphoglycerate; **ACA:** acetyl-CoA; **AKG:** α-ketoglutarate; **ALA**: alanine; **CIT:** citrate; **DHIV**: 2,3--dihydroxy-isovalerate; **IBA**: isobutyraldehyde; **IVA**: isovaleraldehyde; **KIC**: α-ketoisocaproate; **KIV**: α-ketoisovalerate; **LEU**: leucine; **MAL**: malate; **OAA**: oxaloacetate; **PEP**: phosphoenolpyruvate; **PYR**: pyruvate; **SUC**: succinate; **VAL**: valine.

Additionally, pyruvate is the direct precursor of the proteinogenic amino acids alanine, valine, leucine, and isoleucine. In metabolic engineering of cyanobacteria, pyruvate has found use as a major precursor for production of several biofuels and biochemicals (Angermayr et al. 2015). A brief review of two more pyruvate derivatives and metabolic engineering efforts applied towards increasing productivity in cyanobacteria was provided in the Literature Review in Chapter 2.

Pyruvate is formed by pyruvate kinase (PYK) as the final step of glycolysis. PYK catalyzes conversion of phosphoenolpyruvate (PEP) to pyruvate. High levels of ATP, produced in abundance during photosynthesis, have been found to inhibit PYK activity (Knowles et al. 2001). Decreased PYK flux has been observed *in vivo* by an isotopically nonstationary metabolic flux analysis (INST-MFA) of the cyanobacterium *Synechocystis* sp. PCC 6803 under photoautotrophic conditions (Young et al. 2011). In the analysis, a natural PYK bypass was noted in which carbon was channeled from PEP into pyruvate through a three-step pathway involving PEP carboxylase (PEPC), malate dehydrogenase (MDH), and malic enzyme (ME) (Figure 4.1a). Based on the INST-MFA results, a comparable amount of pyruvate was produced through this bypass rather than through PYK (5.3 ± 0.8 moles of ME flux per 100 moles of CO_2 assimilated versus 9.5 ± 0.8 mol of PYK flux per 100 mol CO_2). A more recent analysis performed in wild-type *S. elongatus* also noted higher carbon flux through PEPC, MDH, and ME rather than through PYK (Figure 4.2) (Jazmin 2015). Carbon flux from PEP was significantly greater through PEPC (0.189 ± 0.009 mmol gDW^{-1} h^{-1}) than through PYK (0.004 ± 0.003 mmol gDW^{-1} h^{-1}). Flux into pyruvate from ME (0.023 ± 0.015 mmol gDW^{-1} h^{-1}) was also five times greater than flux from PYK. This bypass provides a potential method for increasing flux to pyruvate, benefitting subsequent production of its derivatives.

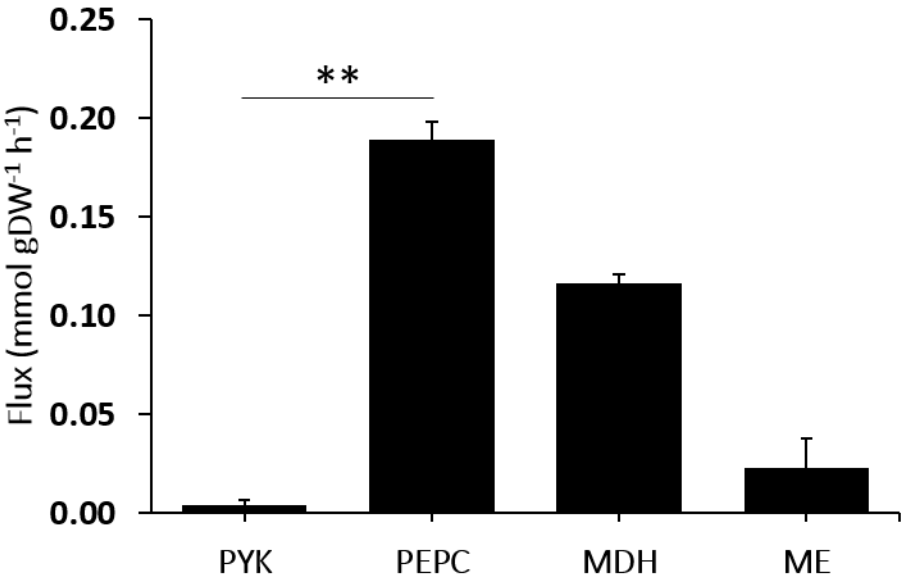

Figure 4.2 – Comparison of flux into pyruvate. The combination of PEP carboxylase (PEPC), malate dehydrogenase (MDH), and malic enzyme (ME) form a natural pyruvate kinase (PYK) bypass to increase carbon flux to pyruvate. ^{13}C MFA analysis of *S. elongatus* was used to estimate the flux through each enzyme. Data ± SEM; n = 3; **p < 0.01.

The IBA-producing cyanobacteria have been engineered through overexpression of each bypass pathway gene: PEPC, MDH, and ME (Table 4.1). For comparison, the PYK enzyme has also been overexpressed within the IBA-producing strain. This set of single-gene overexpression strains comprise the initial set for characterization. The strains showing the greatest increase in IBA production compared to the base strain will be selected as the background for double- and triple-gene overexpressions with the objective of maximizing carbon flux within this bypass pathway to increase flux to pyruvate and, ultimately, IBA.

Method

Culture conditions. Experiments were performed with three biological replicates per strain in BG11 media[1] modified with the addition of 50 mM $NaHCO_3$. Each strain was inoculated to a starting optical density (OD_{750nm}) of 0.4 in 75 mL. Temperature was maintained at 30°C in a water bath on a platform shaker set to 130 rpm. To begin, the cultures were placed in the dark to synchronize the circadian rhythm of the cells. Flasks were removed from the dark after 12 hours and returned to the water bath under a light intensity of 150 $\mu E\ m^{-2}\ s^{-1}$. The cultures were induced with 1 mM isopropyl-beta-D-thiogalactopyranoside (IPTG) to begin expression of the introduced genes. Measurements began six hours after induction.

Strain construction. The base IBA-producing strain was obtained from the lab of James Liao in University of California – Los Angeles. Further engineering was performed by Yao Xu and Lara Jazmin of Vanderbilt University. Each enzyme for overexpression was cloned into a vector encoding carbenicillin resistance. Genes were placed under control of the promoter lacP for

[1] BG-11 medium contains the following per 1 L of deionized water: 1.5 g $NaNO_3$, 0.04 g K_2HPO_4, 0.075 g $MgSO_4$, 0.036 g $CaCl_2$, 0.012 g $FeNH_4$, 0.001 g Na_2EDTA, 0.02 g Na_2CO_3, and 1 mL of trace element mix A_5 [2.86 g L^{-1} H_3BO_3, 1.81 g L^{-1} $MnCl_2$, 0.222 g L^{-1} $ZnSO_4$, 0.391 g L^{-1} Na_2MoO_4, 0.079 g L^{-1} $CuSO_4$, 0.0494 g L^{-1} $Co(NO_3)_2$].

Table 4.1 – Strain list.

Strains	Description	Source
WT	Wild-type *Synechococcus elongatus* sp. PCC 7942	C. Johnson[a]
IBA	Isobutyraldehyde-producing strain. P_{trc}::kivd in NS I ($Spec^R$), $P_L lacO_1$::alsS-alvC-alvD in NS II (Km^R)	(1)
IBA/PYK	Overexpression of pyruvate kinase in NS III (Cb^R) of IBA	Present study
IBA/PEPC	Overexpression of phosphoenolpyruvate carboxylase in NS III (Cb^R) of IBA	Present study
IBA/MDH	Overexpression of malate dehydrogenase from *Synechocystis* sp. PCC 6803 in NS III (Cb^R) of IBA. Codon optimized for *S. elongatus*	Present study
IBA/ME	Overexpression of malic enzyme in NS III (Cb^R) of IBA	Present study

Strains were created by Yao Xu[a] and Lara Jazmin[b].
[a]Department of Biology and Microbiology, Vanderbilt University, Nashville, TN.
[b]Department of Chemical and Biomolecular Engineering, Vanderbilt University, Nashville, TN.
(1) Atsumi et al. 2009

induction by IPTG. Upon selective pressure, the cells incorporated the plasmids into their chromosome, resulting in a stable recombination. The genes encoding malic enzyme and phosphoenolpyruvate carboxylase were cloned from wild-type *S. elongatus*. Malate dehydrogenase was obtained from *Synechocystis* sp. PCC 6803 and codon optimized for insertion into the *S. elongatus* strain.

Growth experiments. Growth was monitored over a 48-hour period during the exponential growth phase. The time period was chosen to encompass at least one doubling time. Rates were calculated using the MATLAB-based software package called ETA (Extracellular Time-course Analysis) (Murphy and Young 2013) and compared to wild-type *S. elongatus*. Significant decreases in growth rate of the engineered strains compared to the controls indicated increased metabolic burden.

Quantification of aldehydes. IBA and IVA were readily stripped from the liquid culture due to their high volatility. Air was bubbled into rubber stoppered culture flasks, and the effluent was condensed in a series of two cold traps containing 25 mL of 1,2-propanediol. The first trap was placed on ice to condense water from the vapor; the second was placed in a chiller set to -28°C. Samples were taken from the traps and analyzed in a gas chromatograph with flame ionization detector (GC/FID)[2] with 1 mM n-butyraldehyde (nBA) added as an internal standard to determine aldehyde concentration. The parent IBA-strain served as the primary control while a wild-type *S. elongatus* was used as a negative control.

Metabolite pool size measurements. Thirty hours after induction, a sample of 20 mL of culture was drawn, rapidly added to a chilled PBS solution to quench metabolism, and placed on

[2] The samples were run using a Shimadzu Scientific Instrument GC 2010 equipped with a DB-Wax column (Agilent Technologies; 30 m x 0.20 μm x 0.20 mm ID). Temperatures were as follows: injection temperature, 210°C; detector temperature, 250°C; column oven temperature program, 30°C for 6 minutes, ramp 30°C min^{-1} to 230°C then hold 6 minutes. Carrier gas used was helium. Injection volume was 0.5 μL using a split ratio of 10:1.

ice. Cells were pelleted out of solution and lysed to extract the intracellular metabolites. The polar metabolites were first derivatized by dissolution in a methoxyamine (MOX; Pierce, Rockford, IL) reagent. Following sonication and incubation, samples were reacted with N,O-bis(trimethylsilyl)trifluoroacetamide (BSTFA) + 10% trimethylchlorosilane (TMCS) for further derivatization and incubated overnight. Samples were then centrifuged to remove further dissolved residue and analyzed using GC/MS[3], using norvaline as an internal standard for comparison among strains.

Results and Discussion

Strain characterization was accomplished by comparing carbon flux into two primary sinks, biomass and aldehydes. Flux into biomass formation was measured as growth rate. Introduction of new carbon-consuming pathways was expected to result in decreased growth as carbon is redirected from biomass. However, among the strains, there was no significant difference in growth rates (Figure 4.3). The average doubling time of 34 hours was higher than the reported value of less than 14 hours in the same strain (Kuan et al. 2015). This was likely an effect of the higher starting cell density in the batch culture (OD ≅ 0.4) resulting in self-shading of the photoautotrophic cells. Comparison of growth rates in a six-day experiment that began at lower cell densities (OD ≅ 0.05) supported this conclusion (Appendix A.3). The parent IBA-producing strain trended towards slower growth ($\mu = 0.0203 \pm 0.0012\ h^{-1}$) in comparison to the wild-type (WT) *S. elongatus* strain ($\mu = 0.0239 \pm 0.0012\ h^{-1}$). The remaining mutant strains exhibited growth rates more consistent with the parent IBA-producing strain. The lowered rate suggests that less

[3] Samples were run using an Agilent Technologies 7890 gas chromatograph equipped with a DB-35MS column (Agilent; 30 m x 0.25 mm x 0.25 mm ID). Temperatures were as follows: injection temperature, 270°C; column oven temperature program, 80°C for 5 minutes, ramp at 10°C min^{-1} to 320°C then hold 5 minutes. Carrier gas used was helium. Injection volume was 1 μL, and samples were run in splitless mode.

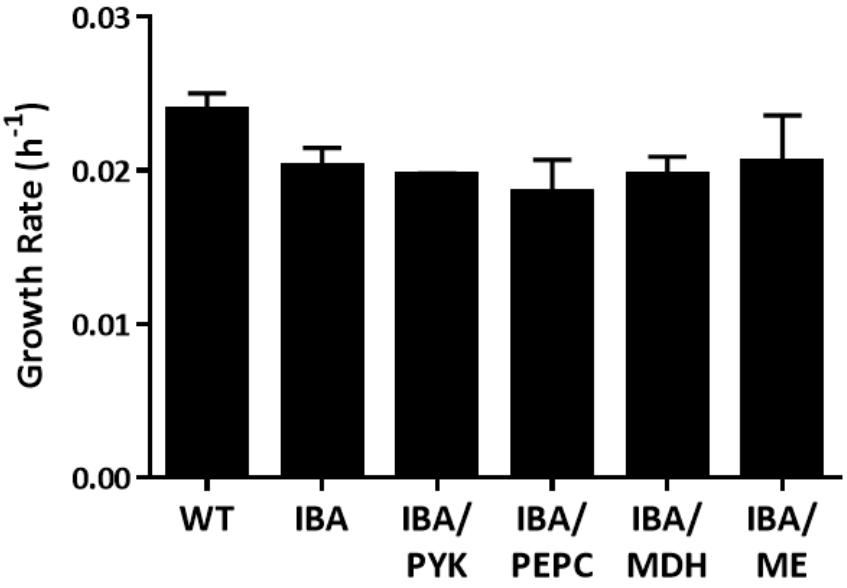

Figure 4.3 – Effect of strain engineering on growth. Growth was tracked by measuring optical density over forty-eight hours following gene induction using 1 mM IPTG. Wild-type *S. elongatus* served as control. Data ± SEM; $n \geq 6$.

carbon was fixed into biomass, consistent with carbon diversion into aldehyde synthesis.

GC/FID was used to quantify flux into aldehyde production over time. As previously mentioned, KIVD facilitated the production of two volatile aldehydes, IBA and IVA. Capture of these aldehydes was achieved by bubbling humidified air through rubber stoppered flasks and into a series of two solvent-filled traps (Appendix B.1). The sum of IBA and IVA was compared among the engineered strains, using the parental IBA-producing strain as the control (Figure 4.4). Overexpression of ME resulted in increased aldehyde productivity (1.2-fold increase relative to the parental IBA-producing strain). This enzyme served as the final, committed step in pyruvate synthesis through the bypass, pulling carbon into pyruvate and, ultimately, IBA. The increased production observed upon overexpression suggested that ME was the rate-determining enzyme within the PYK bypass.

Another characterization tool employed to compare the strains was observing the pool sizes of intracellular metabolites. Pool size measurements provided useful information regarding intracellular flux. Accumulations and depletions in pathway intermediates were used to identify enzymes with low and high conversion rates, respectively, and also to identify downstream bottlenecks. For this experiment, cells were grown in liquid culture for thirty hours in constant light before sampling and rapidly quenching metabolism. The intracellular metabolites were then extracted and derivatized to quantify the pool sizes using GC/MS. Metabolites were selected to show carbon distribution around the pyruvate node and the TCA cycle. The pool sizes of key metabolites within this lower portion of central carbon metabolism were quantified for WT, the parental IBA-producing strain, and the four engineered strains. Figure 4.5 shows the pool sizes of six metabolites, each normalized to an internal standard, norvaline, and expressed relative to the WT strain.

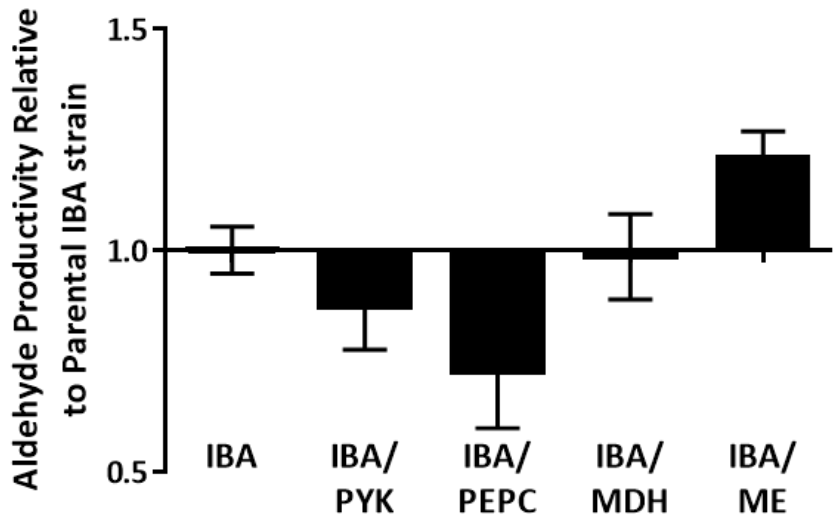

Figure 4.4 – Effect of enzyme overexpression on aldehyde production. Isobutyraldehyde and isovaleraldehyde were captured for 24 hours after induction with 1 mM IPTG and quantified using GC/FID. The total aldehyde productivity from each flask was normalized to the average productivity of the parental IBA-producing culture. Data ± SEM; n ≥ 6.

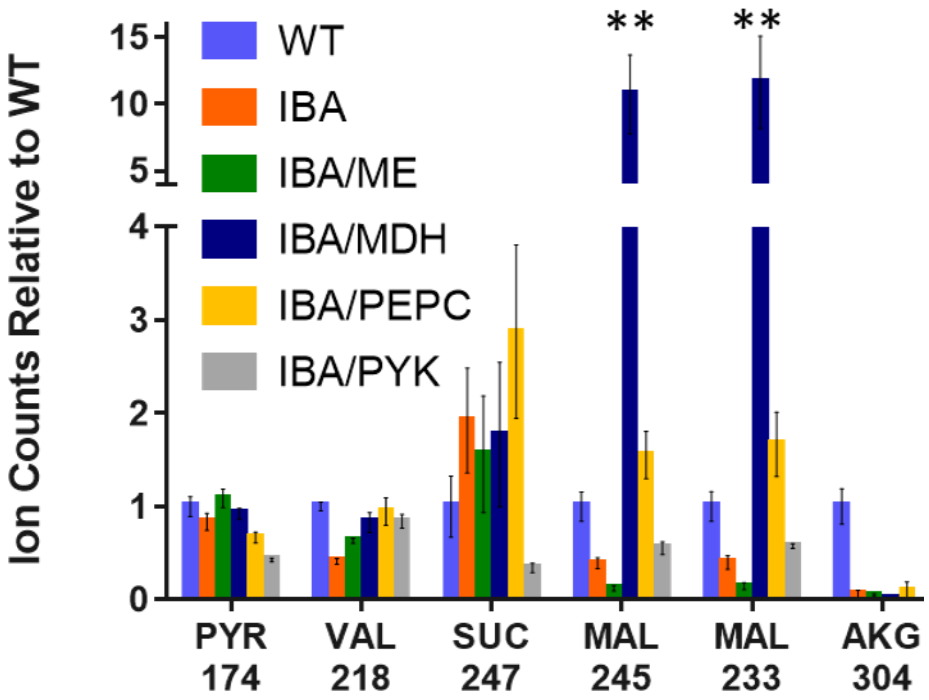

Figure 4.5 – Intracellular pool sizes of pyruvate derivatives. The fragment ion counts of metabolites derivatized by MOX and TMS were quantified using GC/MS. Abbreviations: **AKG**: α-ketoglutarate; **MAL**: malate; **PYR**: pyruvate; **SUC**: succinate; **VAL**: valine. Data ± SEM; n = 4; **p < 0.01.

Overexpression of PEPC, MDH, and ME showed preferential accumulation of metabolites within the reductive branch of the TCA cycle. Cyanobacteria have an incomplete TCA cycle as their genome does not encode the enzyme α-ketoglutarate dehydrogenase to catalyze conversion of α-ketoglutarate (AKG) to succinate (SUC) (Figure 4.1). The reductive branch of the cycle includes the MDH enzyme and terminates in SUC. The pool size of SUC showed a 1.5-fold to 3-fold increase in the parental IBA-producing strain and in strains overexpressing the PYK bypass genes. This suggested that increased carbon entering the reductive branch of the TCA cycle proceeded down the pathway to SUC rather than cycling up to pyruvate. Conversely, overexpressing PYK decreased flux from PEP into this branch, as evidenced by the 65% decrease in the SUC pool size with respect to WT and 80% decrease with respect to the parent IBA-producing strain.

Malate (MAL) was another metabolite within the reductive branch that exhibited a significant difference in pool size. In the MDH-overexpressing strain, the two MAL fragments showed greater than 10-fold and 11-fold increases relative to the WT pool size (Figure 4.5). This showed that MDH overexpression was successful in increasing carbon flux into MAL but unable to increase flux into pyruvate. Conversely, 8-fold and 6-fold decreases were observed for the fragments in the ME overexpression strain. These values identify ME as a pivotal enzyme within the bypass pathway. This provides a physiological explanation as to why ME increased IBA production and verifies the potential of the PYK bypass in increasing productivity of pyruvate derivatives.

Conclusions

An alternate pathway was suggested and tested for increasing pyruvate. Successful increase in pyruvate production was expected to increase production of pyruvate derivatives, IBA and IVA.

Single gene overexpression identified the rate-determining enzyme as ME. Overexpression of ME resulted in depletion of the MAL pool into pyruvate for increased IBA formation. This provided verification of the potential of this PYK bypass pathway for increasing formation of pyruvate derivatives.

CHAPTER V

CONCLUSION

Summary

This thesis has focused on the application of metabolic engineering towards improving the industrial potential of cyanobacteria. The chapters detail methods of analyses using MFA and strain characterization. In this work, these methods were used to determine the metabolic phenotype of different strains and to identify targets for further genetic engineering. The validated analysis methods provide an effective toolset for subsequent strain engineering.

Chapter 3 discussed the simulation results of an INST-MFA application to cyanobacteria. The goal was to determine a minimal data set that could be introduced to the computational program and yield a reliable flux estimation. The metabolites that were found to exert the greatest influence on the model were the substrates and products of the enzymes studied. Time points approaching steady-state labeling most significantly affected the flux reliability, decreasing uncertainty. Using this information, a minimal set of data was tested using simulated data and experimental data (Appendix A). The analysis verified that the minimal set could be used to estimate model fluxes. However, it also highlighted the benefit of a broader set, that is, to increase the certainty and reliability of the flux estimation.

Chapter 4 provided data on the characterization of strains engineered to produce aldehydes. The previous MFA analysis highlighted a bottleneck in production of pyruvate, the major metabolite precursor, as evidenced by comparable flux through a bypass pathway. Each gene within the bypass pathway was overexpressed to determine its effect on carbon flux towards

product. The malic enzyme overexpressing strain showed increased aldehyde productivity over the base strain and was shown to deplete the precursor pool in favor of pyruvate formation. The characterization results indicated potential targets for further genetic engineering.

Recommended Future Works

To further increase aldehyde productivity, the bypass genes, PEPC, MDH, and ME, may be overexpressed in combination. Of the possible pairwise combinations, co-expression of ME and MDH shows the most potential to improve productivity. From Chapter 4, it was observed that MDH overexpression increased the malate pool while ME overexpression depleted it, suggesting that, in combination, these enzymes could significantly increase pyruvate production. Conversely, MDH-PEPC shows the least potential and will likely lead only to malate pooling, as observed in overexpression of MDH. Overexpression of all three genes would be anticipated to increase aldehyde production most significantly.

Exploration of productivity in cyanobacteria would benefit from metabolic flux analyses of the overexpression strains characterized in this work. As discussed in the literature reviews, MFA has been seldom applied to autotrophic cells. Only three articles have been published applying INST-MFA to cyanobacteria (Hasunuma et al. 2013; Huege et al. 2011; Young et al. 2011) with only Young et al. yielding a flux map. INST-MFA of the ME-overexpressing strain can be used to verify the conclusions derived from the metabolite pool study experiment. It may also serve to identify pathways that could be knocked down or deleted to further increase carbon for product formation.

Conclusion

This project addressed one of two primary drawbacks for implementation of cyanobacteria, that is, productivity. However, further improvements can and should be made in this respect. Continuous efforts towards building the cyanobacteria toolset will prove beneficial in increasing its industrial feasibility. Justification for this exploration is that use of cyanobacteria has the potential (i) to decrease dependence on nonrenewable resources, including crude oil, (ii) to decrease side effects on the agricultural industry, resulting from use of arable land and consumable feedstocks, and (iii) to reduce carbon dioxide levels in the atmosphere, reversing effects of parallel industries. Cyanobacteria certainly illustrate potential, and industry will greatly benefit from continued exploration in this regard.

APPENDIX A

SUPPLEMENTAL DATA

Minimal Data Set for INST-MFA

The conclusion from the simulation experiment was that (i) the substrates and products should be included where possible, especially in cyclic or branched pathways and that, (ii) for time points, a reliable flux estimation may be generated using only the initial time point and three time points approaching steady-state enrichment. For verification, these criteria were applied to the *Synechocystis* model using the simulated data as well as the experimental data. Actual experimental error values were used for the experimental data set whereas the error for the simulated data was set to 0.5 mol%. Seven metabolites were initially selected, but an eighth metabolite was needed to bound the confidence intervals for the experimental data (Table A.1). Four time points were chosen as suggested (Figure A.1). As shown in Figure A.2, there is good agreement between the best fit and optimized minimal set with only a slight increase in the confidence interval. The flux estimate values did change in the case of the minimal set using experimental data. However, the best fit values for each flux were still within the confidence interval of the estimated fluxes, indicating that these values may be improved to the correct value by increasing the number of data points.

Table A.1 – Minimal subset of metabolites for INST-MFA.

Metabolite	Group	Related Flux
G6P	oxPPP (G6)	G6PDH
3PGA	CBB-3C/6C (G1)	RBC
RUBP	CBB-5C/7C (G2)	RBC/RBCOX
S7P	CBB-5C/7C (G2)	SBP
GA	PR (G5)	RBCOX
MAL	PEP-cyc (G4)	ME/MS
CIT	TCA (G3)	ME
DHAP*	CBB-3C/6C (G1)	SBP

Seven metabolites were chosen to test if there is a minimal set using which will result in a reliable initial flux estimate. *An eighth metabolite, DHAP, was found necessary to bound the confidence interval of SBP. The group numbers correlate with Table 3.2. Abbreviations: **3PGA**: 3-phosphoglycerate; **CIT**: citrate; **DHAP**: dihydroxyacetone phosphate; **G6P**: glucose-6-phosphate; **G6PDH** glucose-6-phosphate dehydrogenase; **GA**: glycerate; **MAL**: malate; **ME**: malic enzyme; **MS**: malate synthase; **RBC**: ribulose-1,5-bisphosphate carboxylase; **RBCOX**: ribulose-1,5-bisphosphate oxygenase; **RUBP**: ribulose-1,5-bisphosphate; **S7P**: sedoheptulose-7-phosphate; **SBP**: sedoheptulose-1,7-bisphosphatase.

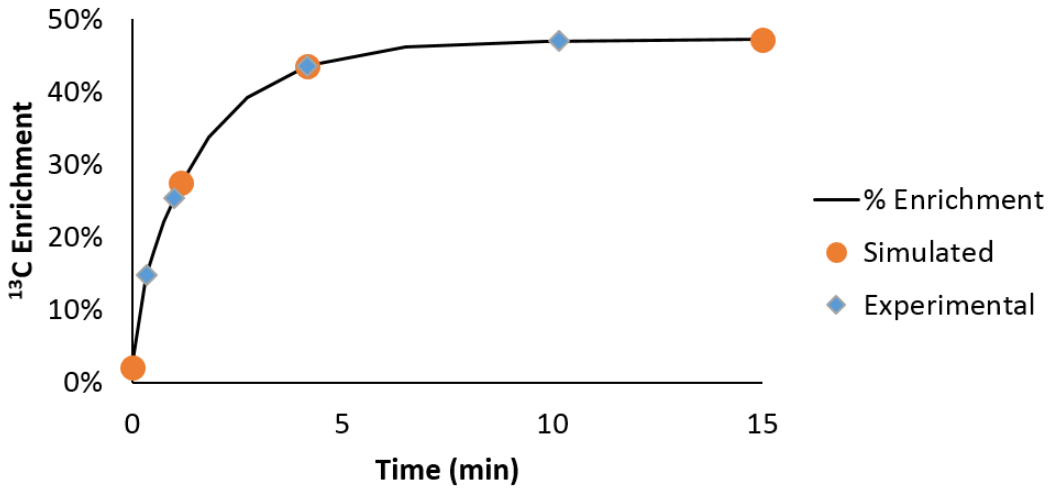

Figure A.1 – Minimal subset of time points for INST-MFA. Time points chosen include the initial time point (0 min. for the simulated data, 0.3333 min. for the experimental data) and time points approaching steady state. In the absence of a 4.1667 min. time point for the experimental data, an 8 min. time point was used.

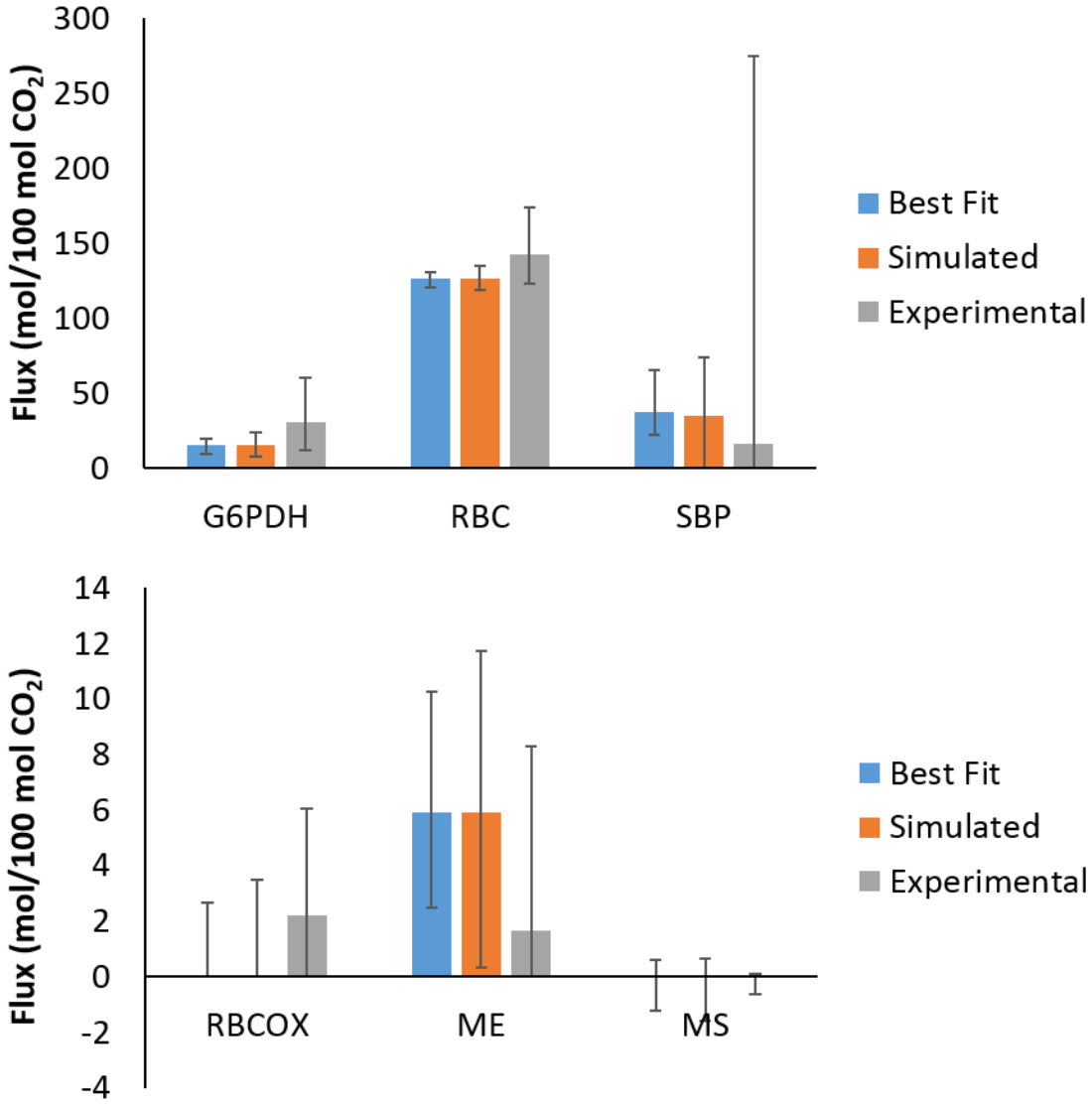

Figure A.2 – INST-MFA fluxes calculated using a minimal subset of inputs. Fluxes were estimated using the metabolites listed in Table A.1 and time points shown in Figure A.1 and compared to the best fit model. Data = value ± 95% confidence interval.

Light-dependent Growth Rate

An optimized growth rate of *Synechococcus elongatus* sp. PCC 7942 was most recently reported as $\mu = 0.052\ h^{-1}$ by Kuan et al. (2015), yet the growth rates determined within experiments performed for this thesis were consistently $\mu \cong 0.020\ h^{-1}$. The primary difference that was investigated was initial culture densities as this effects light availability. Because cyanobacteria are photoautotrophic, it followed that more dense cultures, which resulted in increased self-shading of the cells, would exhibit lower growth rates. To verify that this was, in fact, the source of the observed decrease, the growth rates from the 48-hour curves (Figure 4.3) were compared to growth rates calculated from a 6-day growth curve (Figure A.3). The rates were calculated based on the change in cell density between days 0 – 2 (low density, high light availability) and days 4 – 6 (high density, low light availability). The initial growth rate (D0-2) was nearer the optimal value ($\mu \cong 0.048\ h^{-1}$) while the latter growth rate agreed with the 48-hour growth rates. The cell density range used in the 48-hour growth experiment was chosen to correlate with other experiments requiring high cell density, so these conditions will continue to be used for a more consistent comparison.

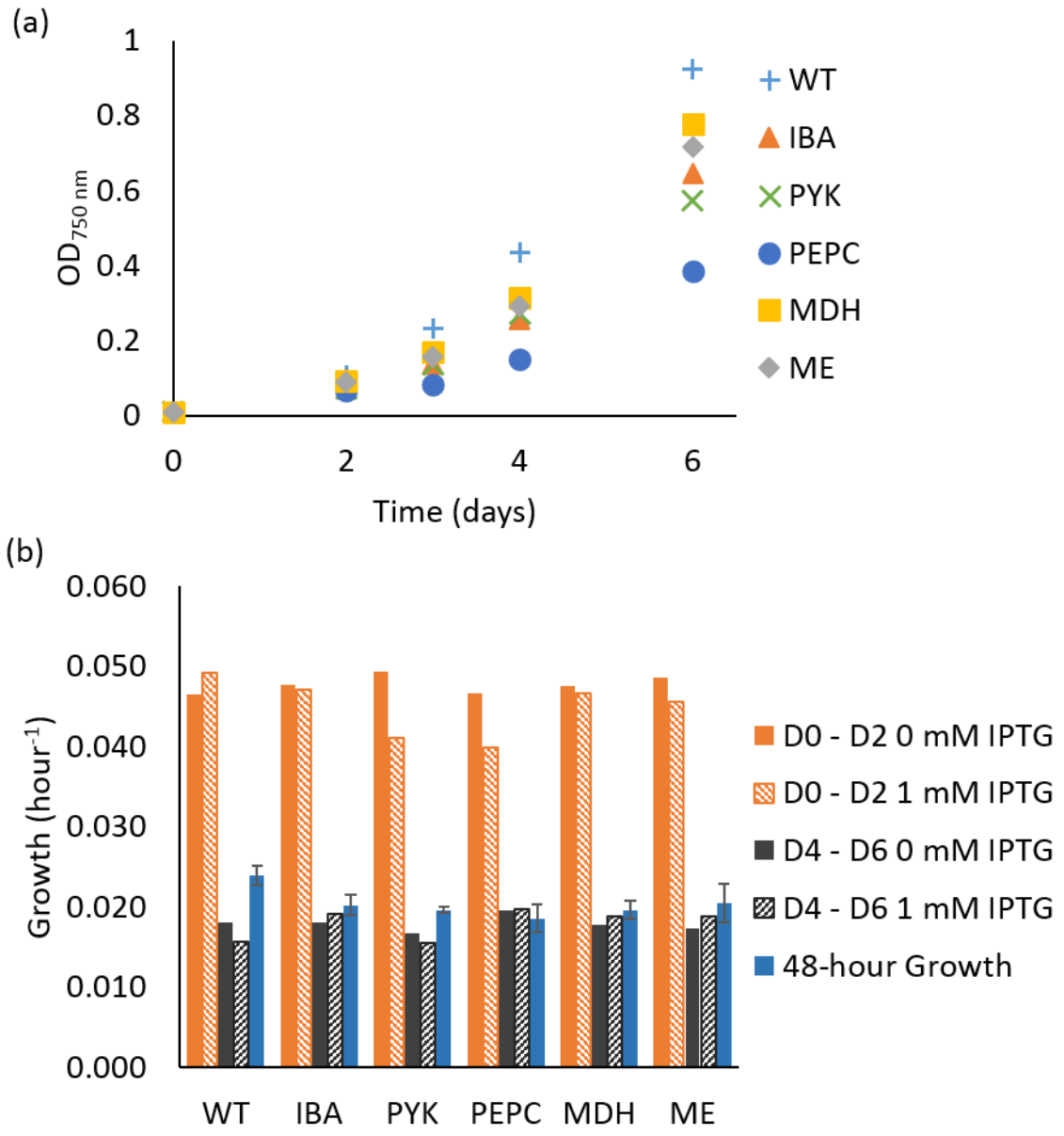

Figure A.3 – Comparison of growth rates during different segments of cell exponential growth. (a) Cell growth was tracked over a period of six days for cultures of wild-type *Synechococcus elongatus* sp. PCC 7942 and the five engineered strains to determine the long term effect of the additional genes on biomass formation. IPTG was added to a final concentration of 1 mM at day 0 for all flasks. n = 1; data obtained from Yao Xu (Department of Biological Sciences, Vanderbilt University). **(b)** Growth rates, μ, were determined assuming exponential growth, $X = X_o \exp(\mu t)$, where X_o was the initial concentration of cells and X was the concentration of cells (OD) at time t. Values calculated from the 6-day growth curves (with and without IPTG, n = 1) were compared to the values calculated from the 48-hour growth curves (Data ± SEM; n ≥ 6).

APPENDIX B

PROTOCOLS

Media Recipes

The two types of media used for cell culturing were BG11 media and LB agar plates. BG11 media was used for agar plates for culture growth from frozen stock and long term growth of strains and also for liquid cultures. To the plates and the pre-culture liquid flasks were added antibiotic resistance to maintain selective pressure on the added genes and to minimize culture contamination. LB plates were used check for contaminations following experiments.

BG11 recipe

- Add make up water to desired 2+ L flask or 1 L media bottle (991.5 mL/L for plate, 983 mL/L for liquid culture).
- Add media components from stock as described below.

		Stock	**Agar Plate**	**Liquid Culture**
1)	$NaNO_3$	150 g/L	5 mL/L	10 mL/L
2)	$K_2HPO_4 \cdot 3H_2O$	40 g/L	0.5 mL/L	1 mL/L
3)	$MgSO_4 \cdot 7H_2O$	75 g/L	0.5 mL/L	1 mL/L
4)	$CaCl_2 \cdot 2H_2O$	36 g/L	0.5 mL/L	1 mL/L
5)	$FeNH_4$•Citrate	12 g/L	0.5 mL/L	1 mL/L
6)	Na_2EDTA (pH8.0)	1 g/L	0.5 mL/L	1 mL/L
7)	Na_2CO_3	20 g/L	0.5 mL/L	1 mL/L
8)	A_5 (listed below)	---	0.5 mL/L	1 mL/L

H_3BO_3	2.86 g/L
$MnCl_2 \cdot 4H_2O$	1.81 g/L
$ZnSO_4 \cdot 7H_2O$	0.222 g/L
$Na_2MoO_4 \cdot 2H_2O$	0.391 g/L
$CuSO_4 \cdot 5H_2O$	0.079 g/L
$Co(NO_3)_2 \cdot 6H_2O$	0.0494 g/L

9) Bacteriological Agar (for Agar only) 15 g/L
10) NaS_2O_3 (for Agar only) 1M 1 mL

- Autoclave on liquid cycle. Allow to cool to touch before proceeding.
- For agar plates:
    - Once cool to touch, add antibiotics to the following concentrations:

Antibiotic	Stock	Final Concentration	Added from stock
Km	50 mg/mL	10 μg/mL	0.2 mL/L
Spec	40 mg/mL	40 μg/mL	1 mL/L
Cb	10 mg/mL	5 μg/mL	0.5 mL/L

    - Pour ~25-30 mL of agar into each sterile petri dish. Allow agar to solidify in hood with open or cracked lids. When cool, replace each lid and store at room temperature.
- For liquid plates:
    - Once cool to touch, $NaHCO_3$ may be added. Remove ~50 mL/L of media into a separate beaker. Add necessary amount of $NaHCO_3$ to smaller volume (4.2 g/L) and mix until fully dissolved. Using a single-use sterilized syringe and 0.20 μm filter, filter sterilize the solution back into the media.

<u>LB media</u>

- Add 500 mL of water to a 1 L Erlenmeyer flask.
- Add the following dry ingredients:
    - 5 g NaCl
    - 5 g Tryptone
    - 2.5 g Yeast Extract
    - 7.5 g Bacteriological agar

- Autoclave on liquid cycle. Allow to cool to touch before proceeding.
- Once cool to touch, pour ~25-30 mL of agar into each plate. Allow agar to solidify in hood with open or cracked lids. When cool, replace each lid and store in 4°C refrigerator.
- Thaw to room temperature before use.

Experiment Preculture

The following protocol provides a method to begin a culture from agar plate for experiment. Consistent use of this method minimizes errors due to different numbers of passages.

- Day 1: Add 2 mL of Modified BG11 media to 5 mL cell culture tube. Inoculate cells from agar plate into media.
- Day 2: Transfer the 2 mL culture to 25 mL of fresh media [with antibiotic, same as above] and place in illuminated (~50 μE m^{-2} s^{-1}) incubator set to 30°C and 100 rpm.
- Day 4-5: Add 25 mL culture to 100 mL of fresh media [with antibiotic] in water bath set to 150 μE m^{-2} s^{-1}, 30°C and 130 rpm, bubbling with air. Grow until the optical density ($OD_{750\ nm}$) is between 0.8 – 1.0.
- When desired OD is reached, begin prep for experiment.

Measuring Optical Density

Optical density (OD) is primarily used to track growth of the culture by measuring the changes in absorbance in the liquid. OD may be converted to concentration of cells using two equations:

Cell density (mg/mL) = $0.684 * (OD_{750} - 0.045) = 0.652 * (OD_{730} - 0.044)$

- Into each well of a 96-well clear bottom plate, pipette 200 μL of liquid.
- Using the μQuant Spectrophotometer, measure absorbance (OD) at 750 nm and 730 nm.
    - For measurements using BG11 media, correct using blank values of 0.045 for OD_{750} and 0.044 for OD_{730}.

Culture Preparation

The culture preparation is consistent for each experiment. Cyanobacteria exhibit a consistent circadian rhythm, or metabolic response to temporal oscillations in light availability. It has been found that this persistent rhythm may be unsynchronized between cells within the same culture. To synchronize the cells to the same rhythm, the cultures are given a 12-hour dark pulse, after which the remaining experiment is performed under constant light.

- Measure OD of preculture flask (dilute 100 μL culture + 900 μL media). Calculate volume needed to inoculate 75 mL of fresh media (V_2) using

$$(CV)_1 = (CV)_2$$

  where C_1 = concentration (OD) of the preculture flask, V_1 = volume (mL) needed to inoculate new culture, C_2 = target OD, and V_2 = volume (mL) of experimental culture.
- Add calculated volume V_1 into each of three (or four, if enough) 50 mL centrifuge tubes and centrifuge at 3000 rpm for 10-12 minutes.
- Remove supernatant.
    - (optional) Resuspend cell pellet in ~5 mL of fresh media and centrifuge again. Remove supernatant.
- Record the weight of the empty flasks.

- Record the weights of the flasks ("before run") filled with desired volume of fresh BG11 media [without antibiotic]. Use 5 ml of media from each flasks to resuspend the cell pellet and return volume to the appropriate flask. Remove 250 μL of culture to measure OD (1 part cells : 2 parts media; 3 x 200 μL per flask).
- For dark pulse, wrap flask completely in foil and place in water bath for twelve hours. (Move clamp rings down, if possible, to prevent tearing the paper.) Turn off lights and record time the flasks were placed in the dark.
- After 12 hours, remove the flasks from the water bath and foil. (Turn the lights back on and replace the rings.)
- Add (V_2 ÷ 1000) μL of 1 M IPTG (final concentration of 1 mM IPTG). Remove 250 μL of culture for measuring OD (1 part cells : 2 parts media; 3 x 200 μL per flask). Return flasks to water bath and begin experimental time line (hour 0).

Determining Cell Growth Rate

Growth rate was tracked over a period of 48 hours to minimize the effect of measurement error or rate calculation. The calculation was accomplished using ETA (Extracellular Time Course Analysis) by inputting ODs averaged over a set of biological replicates, the standard error of the triplicates, and the number of replicates (typically n = 3) (Murphy and Young 2013).

- For growth experiments, use 125 Erlenmeyer flasks sealed with a foam plug (size C) and fitted with a 5 mL plastic pipette (sterile) and 6" autoclaved needle with luer lock attachment.
    - Cover each needle (for example, using 2 mL microcentrifuge tubes or aluminum foil) to prevent contamination.

- Beginning at hour 6 (time 0), remove ~300 μL of culture using sterile 3 mL syringes. Use 250 μL of sample to measure OD (1 part cells : 2 parts media; 3 x 200 μL per flask).
- To capture exponential increase in growth, space time points based on growth equation:

$$\ln X = \ln X_o + \mu t, \text{ or}$$

$$t = \mu^{-1} (\ln X - \ln X_o)$$

Based on these equations, the time points used were as follows:

Time Pts	0	1	2	3	4	5	6	7	8	9	10	11	12
Hour	6	12	17	22	26	30	34	38	42	45	48	51	54

- For use in ETA, compile data into a table in Excel in four separate columns:

Time point	Averaged Values	Standard Deviation	No. of Replicates

Measuring Aldehyde Concentrations

The aldehydes, isobutyraldehyde and isovaleraldehyde, have high vapor pressures, which allow them to be easily stripped from culture. The experimental design modified from Rodriguez and Atsumi (2012) has been designed to take advantage of this property by bubbling the chemicals out and into a series of solvent traps for capture. The traps were placed in subsequently lowered temperatures to ensure condensation of the aldehydes. Samples were taken from the trap and measured using a Shimadzu GC-2010 with Flame Ionization Detector (GC/FID). Aldehyde concentrations were determined by comparison to a calibration curve.

- Flasks should be fitted with rubber stoppers with two glass rods for inlet and outlet flow. Autoclave the entire ensemble together.

- Weigh 2 sets of 50 mL centrifuge tubes empty (with caps). Add 25 mL of 50% propylene glycol to each tube and weigh ("before run"). Place one set of tubes ("Traps X-1") into the ice bucket. Place remaining set into the chiller.
    - If using an ice box that can be prepared beforehand, place the Trap 1 tubes in the ice box and fill with enough water to cover the bottom of the tubes. Place in -20°C freezer. Once frozen, add more water to cover at least half of the tube but leave at least 1" – 2" of space between water and bucket lid (to allow for ice expansion).
- Prepare the centrifuge tubes for the experiment by placing the appropriate caps with inlet/outlet tubing. Connect as shown below (Figure B.1).
- At hour 18 (after induction), measure OD of each culture and connect tubes to flasks. Run for 12 hours.
- Disconnect the apparatus. Measure final OD. Weigh final masses of each trap (with the original caps) and flasks. Place in refrigerator.
- Vortex the traps and allow to settle. Measure out 450 μL from each trap and combine with 5 μL of 100 mM nBA (internal standard; final concentration of 1 mM nBA). Measure out 200 μL into a 2 mL GC amber vial fitted with 250 μL polypropylene insert to run on GC/FID.
- Run on GC/FID alongside a calibration curve to determine the concentration of aldehyde produced.

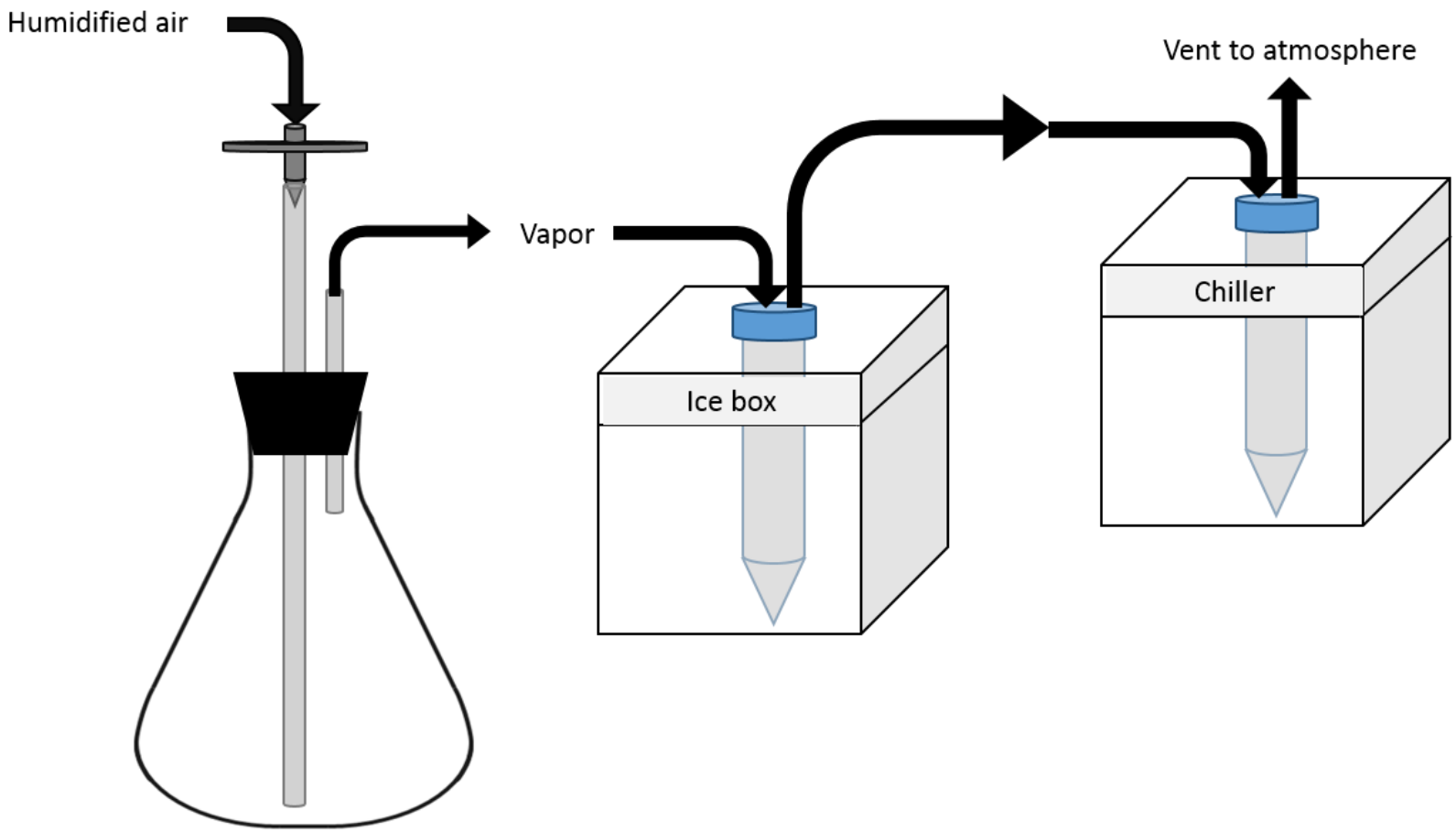

Figure B.1 – Aldehyde trap set up. Each 125 Erlenmeyer flask is plugged with a rubber stopped that is fitted with two glass pipettes, one long and one short. The traps are 50 mL centrifuge tubes filled with 25 mL of propylene glycol. Set 1 (Trap X-1) is placed in an ice box to encourage condensation of water. Set 2 (Trap X-2) is placed in a refrigerated chiller set to less than -20°C for condensing the aldehydes from the vapor phase into solution. Humidified air is bubbled into flasks one and flows as indicated in the image.

Calibration Curve for Aldehyde Quantification

Because GC/FID cannot directly quantify the concentration of a chemical, a calibration curve is run in parallel with the samples for comparison. Beginning with a known concentration of IBA and IVA, serial dilutions are performed. An internal standard n-butyraldehyde (nBA) is added to each standard and each sample to the same final concentration. The ratio between the final area counts of IBA or IVA and nBA of the standards were used to determine a linear regression. The equations of these lines were used to calculate the concentration of aldehyde in the samples.

- Into five 2 mL microcentrifuge tubes, add the start volumes as listed in the table below.
- Create a stock concentration of 200 mM each of IBA and IBA to a single 2 mL microcentrifuge tube using 18.26 µL of IBA, 21.45 µL of IVA, and 960 µL of solvent (50% propylene glycol/water).
- Add 10 µL of 200 mM stock to Tube 1 and dilute the subsequent tubes (2 – 5) to final concentrations as listed.

	1	2	3	4	5
Start Volume	990 µL	900 µL	900 µL	900 µL	800 µL
Dilution volume	-	300 µL	300 µL	300 µL	400 µL
Concentration	2 mM	0.50 mM	0.13 mM	0.03 mM	0.01 mM

- Create a 100 mM nBA stock using 8.83 µL nBA in 991 µL of solvent.
- Remove 495 µL from each tube into a separate 2 mL microcentrifuge tube. Add 5 µL of 100 mM nBA to each tube and vortex.
- Pipette 200 µL from each tube into an amber vial with a 250 µL polypropylene insert to run on the GC/FID.

GC/FID Program

The settings for the Shimadzu GC-2010 with Flame Ionization Detector were as follows:

- Injector temperature: 210°C
- Detector temperature: 250°C
- Column: Agilent Technologies DB-Wax column, 30 m, 0.20 μm film thickness, 0.20 mm ID
- Column oven temperature: 30°C for 6 min, ramp 6°C/min to 60°C, hold 2 minutes, ramp 40°C/min to 220°C, hold 7 minutes
- Injection volume: 0.5 μL
- Carrier gas: Helium
- Column flow: 0.78 mL/min
- Purge flow rate: 0.5 mL/min
- Split ratio: 10:1

Metabolite Pool Size Measurements

Metabolite pool sizes were measured using an Agilent Technologies 7890A GC System with Mass Spectrometer 5975C with Triple-Axis Detector. The experimental timeline was designed to match that of isotopically nonstationary metabolic flux analyses experiments. Area counts for each metabolite of interest were measured and normalized to an internal standard, norvaline. Samples were derivatized using methoxyamine (MOX) and trimethylsilane (TMS) to volatilize the samples of interest and increase the fragment sizes for measurement by GC/MS. Comparison between engineered strains and the wild-type strain highlighted potential bottlenecks and also shifts in fluxes that led to pools in carbon sinks.

Quenching

- Overnight: pre-chill phosphate-buffered saline (PBS; 4°C) for the quenching solution and chloroform and methanol for extraction (-20°C).
- Use 125 Erlenmeyer flasks sealed with a foam plug (size C) and fitted with a 5 mL plastic pipette (sterile) and 6" autoclaved needle with luer lock attachment.
    - Cover each needle (for example, using 2 mL microcentrifuge tubes or aluminum foil) to prevent contamination.
- Aliquot 30 mL of PBS into 50 mL centrifuge tubes.
- At hour 30 (after induction), remove 20 mL of sample from each culture using a 20 mL syringe and quickly add to centrifuge containing chilled PBS. Mix to quench metabolism and place on ice.
- Vortex tubes and centrifuge at 5,000 rpm for 5 minutes at -10°C.
- Aspirate supernatant and flash freeze cell pellet (liquid nitrogen). Store in -80°C freezer until use.

Extracting

- Resuspend cells in 4 mL chloroform (prechilled to -20°C).
- Add 2 mL methanol (prechilled to -20°C) and vortex tubes for 30 minutes in refrigerator.
- Add 1.5 mL iced-cold water, then vortex tubes for additional 5 minutes.
- Transfer to 15 mL centrifuge tube.
- Centrifuge at 5,000 rpm for 20 min at lowest temperature setting.
- Collect aqueous (upper) phase in a new 15 mL tube or two Eppendorf tubes (label the tubes).

    - (optional) Collect organic (lower) phase in a new 15 mL tube or two Eppendorf tubes.
- Evaporate all extracts to dryness using N_2 at room temperature. If using two tubes, evaporate until volume is less than 800 µL; resuspend any dried product on tube walls and combine the contents of one tubes into the other.
    - NOTE: Add internal standard of Norvaline prior to final drying step (if using two tubes, add when combining tubes.)
- Store samples at -80°C until use.

MOX/TMS Derivatization

- Dissolve the dried sample in 50 µL of MOX reagent.
- Place in sonication bath for 30 min. at room temperature.
- Incubate for 90 min. at 40°C on a heating block.
- Add 70 uL of BSTFA +10 % TMCS.
- For TMS: Incubate for 30 min. at 40°C on a heating block.
- Remove from heating block and incubate overnight at room temperature.
- Centrifuge for 5 min at 14,000 rpm to remove solid debris.
- Transfer liquid to 2 mL amber vial with a 250 µL insert.

GC/FID Program

The settings for the Agilent 7890A GC System with Mass Spectrometer 5975C with Triple-Axis Detector were as follows:

- Injector temperature: 270°C
- Column: Agilent Technologies DB-35MS column, 30 m, 0.25 µm film thickness, 0.25 mm ID

- Column oven temperature: 80°C for 5 min, ramp 10°C/min to 320°C, hold 5 minutes
- Injection volume: 1 μL
- Carrier gas: Helium
- Gas flow rate: 1 mL/min
- Purge flow rate: 50 mL/min
- Splitless for 2 minutes
- Mass spectra obtained in scan mode over the range 100 – 500 m/z.

REFERENCES

Adebiyi AO, Jazmin LJ, Young JD (2014) 13C flux analysis of cyanobacterial metabolism. Photosynthesis research:1-14. doi:10.1007/s11120-014-0045-1

Angermayr SA, Gorchs Rovira A, Hellingwerf KJ (2015) Metabolic engineering of cyanobacteria for the synthesis of commodity products. Trends in Biotechnology 33 (6):352-361. doi:10.1016/j.tibtech.2015.03.009

Antoniewicz MR (2013) Using multiple tracers for 13C metabolic flux analysis. Methods Mol Biol 985:353-365. doi:10.1007/978-1-62703-299-5_17

Antoniewicz MR, Kraynie DF, Laffend LA, Gonzalez-Lergier J, Kelleher JK, Stephanopoulos G (2007) Metabolic flux analysis in a nonstationary system: fed-batch fermentation of a high yielding strain of E. coli producing 1,3-propanediol. Metabolic engineering 9 (3):277-292. doi:10.1016/j.ymben.2007.01.003

Atsumi S, Higashide W, Liao JC (2009) Direct photosynthetic recycling of carbon dioxide to isobutyraldehyde. Nat Biotech 27 (12):1177-1180. doi:10.1038/nbt.1586

Billig E (2000) Butyl Alcohols. In: Kirk-Othmer Encyclopedia of Chemical Technology. John Wiley & Sons, Inc. doi:10.1002/0471238961.0221202502091212.a01.pub2

Deng MD, Coleman JR (1999) Ethanol synthesis by genetic engineering in cyanobacteria. Applied and environmental microbiology 65 (2):523-528

Dexter J, Fu P (2009) Metabolic engineering of cyanobacteria for ethanol production. Energy & Environmental Science 2 (8):857-864. doi:10.1039/B811937F

Ducat DC, Sachdeva G, Silver PA (2011) Rewiring hydrogenase-dependent redox circuits in cyanobacteria. Proceedings of the National Academy of Sciences of the United States of America 108 (10):3941-3946. doi:10.1073/pnas.1016026108

Dutta D, De D, Chaudhuri S, Bhattacharya S (2005) Hydrogen production by Cyanobacteria. Microbial Cell Factories 4 (1):36

Gao Q, Wang W, Zhao H, Lu X (2012) Effects of fatty acid activation on photosynthetic production of fatty acid-based biofuels in Synechocystis sp. PCC6803. Biotechnology for biofuels 5 (1):17. doi:10.1186/1754-6834-5-17

Gong F, Liu G, Zhai X, Zhou J, Cai Z, Li Y (2015) Quantitative analysis of an engineered CO2-fixing Escherichia coli reveals great potential of heterotrophic CO2 fixation. Biotechnology for biofuels 8:86. doi:10.1186/s13068-015-0268-1

Hasunuma T, Kikuyama F, Matsuda M, Aikawa S, Izumi Y, Kondo A (2013) Dynamic metabolic profiling of cyanobacterial glycogen biosynthesis under conditions of nitrate depletion. Journal of experimental botany 64 (10):2943-2954. doi:10.1093/jxb/ert134

Hu Q, Richmond A (2013) Handbook of Microalgal Culture : Applied Phycology and Biotechnology (2nd Edition). John Wiley & Sons, Somerset, NJ, USA

Huege J, Goetze J, Schwarz D, Bauwe H, Hagemann M, Kopka J (2011) Modulation of the Major Paths of Carbon in Photorespiratory Mutants of Synechocystis. PLoS ONE 6 (1)

Jazmin LJ (2015) unpublished data.

Jazmin LJ, O'Grady JP, Ma F, Allen DK, Morgan JA, Young JD (2014) Isotopically Nonstationary MFA (INST-MFA) of Autotrophic Metabolism. In: Dieuaide-Noubhani M, Alonso AP (eds) Plant Metabolic Flux Analysis, vol 1090. Methods in Molecular Biology. Humana Press, pp 181-210. doi:10.1007/978-1-62703-688-7_12

Jazmin LJ, Young JD (2013) Isotopically Nonstationary 13C Metabolic Flux Analysis. In: Alper HS (ed) Systems Metabolic Engineering, vol 985. Methods in Molecular Biology. Humana Press, pp 367-390. doi:10.1007/978-1-62703-299-5_18

Kämäräinen J, Knoop H, Stanford NJ, Guerrero F, Akhtar MK, Aro EM, Steuer R, Jones PR (2012) Physiological tolerance and stoichiometric potential of cyanobacteria for hydrocarbon fuel production. J Biotechnol 162 (1):67-74. doi:10.1016/j.jbiotec.2012.07.193

Khoo HH (2015) Review of bio-conversion pathways of lignocellulose-to-ethanol: Sustainability assessment based on land footprint projections. Renewable and Sustainable Energy Reviews 46 (0):100-119. doi:10.1016/j.rser.2015.02.027

Knowles VL, Smith CS, Smith CR, Plaxton WC (2001) Structural and regulatory properties of pyruvate kinase from the Cyanobacterium synechococcus PCC 6301. The Journal of biological chemistry 276 (24):20966-20972. doi:10.1074/jbc.M008878200

Koffas M, Stephanopoulos G (2005) Strain improvement by metabolic engineering: lysine production as a case study for systems biology. Current Opinion in Biotechnology 16 (3):361-366. doi:10.1016/j.copbio.2005.04.010

Kuan D, Duff S, Posarac D, Bi X (2015) Growth optimization of Synechococcus elongatus PCC7942 in lab flasks and a 2-D photobioreactor. The Canadian Journal of Chemical Engineering 93 (4):640-647. doi:10.1002/cjce.22154

Kumar K, Dasgupta CN, Nayak B, Lindblad P, Das D (2011) Development of suitable photobioreactors for CO2 sequestration addressing global warming using green algae and cyanobacteria. Bioresource technology 102 (8):4945-4953. doi:10.1016/j.biortech.2011.01.054

Leighty RW, Antoniewicz MR (2011) Dynamic metabolic flux analysis (DMFA): a framework for determining fluxes at metabolic non-steady state. Metab Eng 13 (6):745-755. doi:10.1016/j.ymben.2011.09.010

Liu X, Sheng J, Curtiss R, 3rd (2011) Fatty acid production in genetically modified cyanobacteria. Proceedings of the National Academy of Sciences of the United States of America 108 (17):6899-6904. doi:10.1073/pnas.1103014108

Masukawa H, Inoue K, Sakurai H, Wolk CP, Hausinger RP (2010) Site-directed mutagenesis of the Anabaena sp. strain PCC 7120 nitrogenase active site to increase photobiological hydrogen production. Applied and environmental microbiology 76 (20):6741-6750. doi:10.1128/aem.01056-10

Murphy TA, Young JD (2013) ETA: robust software for determination of cell specific rates from extracellular time courses. Biotechnology and bioengineering 110 (6):1748-1758. doi:10.1002/bit.24836

Nielsen J (2003) It Is All about Metabolic Fluxes. Journal of Bacteriology 185 (24):7031-7035. doi:10.1128/jb.185.24.7031-7035.2003

Noh K, Gronke K, Luo B, Takors R, Oldiges M, Wiechert W (2007) Metabolic flux analysis at ultra short time scale: isotopically non-stationary 13C labeling experiments. J Biotechnol 129 (2):249-267. doi:10.1016/j.jbiotec.2006.11.015

Nöh K, Wiechert W (2006) Experimental design principles for isotopically instationary 13C labeling experiments. Biotechnology and bioengineering 94 (2):234-251. doi:10.1002/bit.20803

Nozzi NE, Atsumi S (2015) Genome Engineering of the 2,3-Butanediol Biosynthetic Pathway for Tight Regulation in Cyanobacteria. ACS Synthetic Biology. doi:10.1021/acssynbio.5b00057

Oliver JW, Machado IM, Yoneda H, Atsumi S (2013) Cyanobacterial conversion of carbon dioxide to 2,3-butanediol. Proceedings of the National Academy of Sciences of the United States of America 110 (4):1249-1254. doi:10.1073/pnas.1213024110

Oliver JWK, Atsumi S (2015) A carbon sink pathway increases carbon productivity in cyanobacteria. Metabolic Engineering 29 (0):106-112. doi:10.1016/j.ymben.2015.03.006

Piven I, Friedrich A, Dühring U, Uliczka F, Baier K, Inaba M, Shi T, Wang K, Enke H, Kramer D (2014) Cyanobacterium sp. for Production of Compounds. Google Patents,

Quintana N, Van der Kooy F, Van de Rhee MD, Voshol GP, Verpoorte R (2011) Renewable energy from Cyanobacteria: energy production optimization by metabolic pathway engineering. Applied microbiology and biotechnology 91 (3):471-490. doi:10.1007/s00253-011-3394-0

Rodriguez GM, Atsumi S (2012) Isobutyraldehyde production from Escherichia coli by removing aldehyde reductase activity. Microbial Cell Factories 11:90-90. doi:10.1186/1475-2859-11-90

Ryan C, Munz D, Bevers G (2011) Isobutanol-A Renewable Solution for the Transportation Fuels Value Chain. Pipeline stress corrosion cracking (SCC) and elastomeric compatibility

Sauer U (2006) Metabolic networks in motion: 13C-based flux analysis. Molecular Systems Biology 2 (1):n/a-n/a. doi:10.1038/msb4100109

Savakis PE, Angermayr SA, Hellingwerf KJ (2013) Synthesis of 2,3-butanediol by Synechocystis sp. PCC6803 via heterologous expression of a catabolic pathway from lactic acid- and enterobacteria. Metabolic Engineering 20 (0):121-130. doi:10.1016/j.ymben.2013.09.008

Sharma NK, Rai AK, Stal LJ (2013) Cyanobacteria : An Economic Perspective. John Wiley & Sons, Incorporated, Somerset, NJ, USA

Shastri AA, Morgan JA (2007) A transient isotopic labeling methodology for 13C metabolic flux analysis of photoautotrophic microorganisms. Phytochemistry 68 (16-18):2302-2312. doi:10.1016/j.phytochem.2007.03.042

Stephanopoulos G (1999) Metabolic fluxes and metabolic engineering, vol 1. vol 1, 2000/08/10 edn. doi:10.1006/mben.1998.0101

Stephanopoulos G, Aristidou AA, Nielsen J (1998) Metabolic engineering: principles and methodologies. Academic press,

Vallino JJ, Stephanopoulos G (1994) Carbon Flux Distributions at the Pyruvate Branch Point in Corynebacterium glutamicum during Lysine Overproduction. Biotechnology progress 10 (3):320-326. doi:10.1021/bp00027a013

Varman AM, Xiao Y, Pakrasi HB, Tang YJ (2013) Metabolic engineering of Synechocystis sp. strain PCC 6803 for isobutanol production. Applied and environmental microbiology 79 (3):908-914. doi:10.1128/aem.02827-12

Wegner A, Weindl D, Jäger C, Sapcariu SC, Dong X, Stephanopoulos G, Hiller K (2014) Fragment Formula Calculator (FFC): Determination of Chemical Formulas for Fragment Ions in Mass Spectrometric Data. Analytical Chemistry 86 (4):2221-2228. doi:10.1021/ac403879d

Wiechert W (2001) 13C Metabolic Flux Analysis. Metabolic Engineering 3 (3):195-206. doi:10.1006/mben.2001.0187

Woolston BM, Edgar S, Stephanopoulos G (2013) Metabolic engineering: past and future. Annual review of chemical and biomolecular engineering 4:259-288. doi:10.1146/annurev-chembioeng-061312-103312

Yao L, Qi F, Tan X, Lu X (2014) Improved production of fatty alcohols in cyanobacteria by metabolic engineering. Biotechnology for biofuels 7:94. doi:10.1186/1754-6834-7-94

Yoshikawa K, Hirasawa T, Shimizu H (2015) Effect of malic enzyme on ethanol production by Synechocystis sp. PCC 6803. Journal of bioscience and bioengineering 119 (1):82-84. doi:10.1016/j.jbiosc.2014.06.001

Young JD, Shastri AA, Stephanopoulos G, Morgan JA (2011) Mapping photoautotrophic metabolism with isotopically nonstationary (13)C flux analysis. Metab Eng 13 (6):656-665. doi:10.1016/j.ymben.2011.08.002

Young JD, Walther JL, Antoniewicz MR, Yoo H, Stephanopoulos G (2008) An elementary metabolite unit (EMU) based method of isotopically nonstationary flux analysis. Biotechnology and bioengineering 99 (3):686-699. doi:10.1002/bit.21632